International Journal of Extreme Manufacturing

Soft sensory-neuromorphic system for closed-loop neuroprostheses

OPEN ACCESS
IMMT | IOP Publishing
International Journal of Extreme Manufacturing
Int. J. Extrem. Manuf. **7** (2025) 042001 (32pp)
https://doi.org/10.1088/2631-7990/adb9aa

Topical Review

Soft sensory-neuromorphic system for closed-loop neuroprostheses

Jaehyon Kim[1,2,§], **Sungjun Lee**[1,2,§], **Jiyong Yoon**[1,2,§] **and Donghee Son**[1,2,3,4,*]

[1] Department of Electrical and Computer Engineering, Sungkyunkwan University (SKKU), Suwon 16419, Republic of Korea
[2] Center for Neuroscience Imaging Research, Institute for Basic Science (IBS), Suwon, Republic of Korea
[3] KIST-SKKU Carbon-Neutral Research Center, Sungkyunkwan University (SKKU), Suwon 16419, Republic of Korea
[4] Department of Artificial Intelligence System Engineering, Sungkyunkwan University (SKKU), Suwon 16419, Republic of Korea

E-mail: daniel3600@g.skku.edu

Received 10 October 2024, revised 9 December 2024
Accepted for publication 24 February 2025
Published 26 March 2025

Abstract

Prosthetic devices designed to assist individuals with damaged or missing body parts have made significant strides, particularly with advancements in machine intelligence and bioengineering. Initially focused on movement assistance, the field has shifted towards developing prosthetics that function as seamless extensions of the human body. During this progress, a key challenge remains the reduction of interface artifacts between prosthetic components and biological tissues. Soft electronics offer a promising solution due to their structural flexibility and enhanced tissue adaptability. However, achieving full integration of prosthetics with the human body requires both artificial perception and efficient transmission of physical signals. In this context, synaptic devices have garnered attention as next-generation neuromorphic computing elements because of their low power consumption, ability to enable hardware-based learning, and high compatibility with sensing units. These devices have the potential to create artificial pathways for sensory recognition and motor responses, forming a "sensory-neuromorphic system" that emulates synaptic junctions in biological neurons, thereby connecting with impaired biological tissues. Here, we discuss recent developments in prosthetic components and neuromorphic applications with a focus on sensory perception and sensorimotor actuation. Initially, we explore a prosthetic system with advanced sensory units, mechanical softness, and artificial intelligence, followed by the hardware implementation of memory devices that combine calculation and learning functions. We then highlight the importance and mechanisms of soft-form synaptic devices that are compatible with sensing units. Furthermore, we review an artificial sensory-neuromorphic perception system that replicates various biological senses and

§ These authors contributed equally to this work and should be considered co-first-author.
* Author to whom any correspondence should be addressed.

facilitates sensorimotor loops from sensory receptors, the spinal cord, and motor neurons. Finally, we propose insights into the future of closed-loop neuroprosthetics through the technical integration of soft electronics, including bio-integrated sensors and synaptic devices, into prosthetic systems.

Keywords: soft electronics, synaptic devices, sensory-neuromorphic system, closed-loop neuroprosthetics

1. Introduction

Prostheses designed to assist individuals with the absence or impairment of tissues such as nerves, brain, muscles, or sensory receptors have been extensively developed over several decades. Early prosthetic devices, made from wood or pure metals, were primarily constructed to provide structural support[1,2]. However, these early prostheses were physically limited in their ability to support the complex range of movements required for daily life. To address these limitations, prosthetic devices have evolved to incorporate electronic technologies that detect signals such as muscle signals, allowing the device to interpret the user's intentions and adjust accordingly[3−6]. Recent advancements in artificial intelligence (AI), robotics, tissue engineering, and neural engineering have significantly enhanced the performance and convenience of prosthetics[7−15]. Notable studies include the development of data processors and software methodologies capable of handling large volumes of data[7−9], real-time status displays[10−12], and actuators for precise movement[13−15]. Still, most innovations have focused on preprogrammed actuation of robotic motor responses to sensory signals rather than providing realistic perception of external environments or seamless interaction with the human body[16,17]. For user-customized prosthetic devices to function continuously and efficiently as an extension of the human body in daily life, a closed-loop operation of the entire system is required. This system involves continuous feedback between biological tissues (e.g., brain, nerves, and muscles) and electronic components (e.g., robotic motors and displays) to ensure accurate, high-speed, convenient, and low-power operations.

To develop highly accurate and responsive prostheses that enable artificial sensory perceptions and neural interactions, numerous studies have focused on improving the performance of individual components and enhancing interfaces for better integration[18−23]. Sensing units, one of the critical components of prosthetic devices, have been developed in two main trends: (i) improving the quality of sensor data through material and structural innovations[18−20] and (ii) developing software algorithms and hardware fabrications to process data obtained from these sensors[21−23]. In the first strategy, soft sensors are designed to conform to irregular tissue surfaces, enabling bidirectional neural interfaces that capture biological signals and provide electrical stimulation to nerves for robotic control. The second strategy involves exploring the utilization of AI and other advanced software based on deep-learning methods to process complex datasets. As the size of the collected and required information from the sensors increases and becomes complicated, post-processing steps with intelligent algorithms have become essential for the precise control of prosthetics and real-time diagnosis of the user's condition, due to the decoupling of noise signals and customized systems.

Yet, AI-based software faces challenges in hardware implementation, which is crucial for achieving high speed and reducing power consumption in prosthetic systems[24−26]. To address these limitations, researchers have proposed hardware-based processing units that combine calculations and memory functions[27−34]. Conventional in-memory computing devices based on traditional computer architectures, which are based on complementary metal-oxide semiconductors (CMOS), suffer from the von Neumann bottleneck, leading to high power consumption and spatial inefficiency due to the separation of the central processing unit (CPU) and memory devices[27−30]. By mimicking the neurons and synaptic junctions of the brain, neuromorphic computing enables simultaneous computation and storage with significantly reduced power consumption, suggesting a promising solution to these issues[31−34]. This approach has attracted attention in the fabrication of various memory devices, offering superior performance and high scalability from device to chip levels. However, integrating memory-based computing chips with soft sensors remains challenging for prosthetic applications, as these memory units, designed for processing and learning structured datasets, struggle with unstructured and irregular sensory signals from soft sensory units[35−37]. Thus, there is a need for soft, neuro-inspired processing units that efficiently handle biological data while minimizing mechanical mismatches and signal interference with sensory units.

Synaptic devices, which replicate biological synaptic junctions, are promising candidates to address these challenges. In the human body, the transmission, storage, and learning of biological signals are mediated by synapses between neurons (Figure 1(a)). Neurotransmitters are released from presynaptic to postsynaptic neurons through the synaptic cleft, where action potentials are multiplied by analog synaptic weights and summed to generate spike signals[38−43]. Similarly, synaptic devices multiply the voltage input signal by conductance to produce a current signal as the output (Figure 1(b)). These artificial synapses with multiple analog states are highly compatible with analog signals from sensory units, offering low-power computation, and efficient data transmission

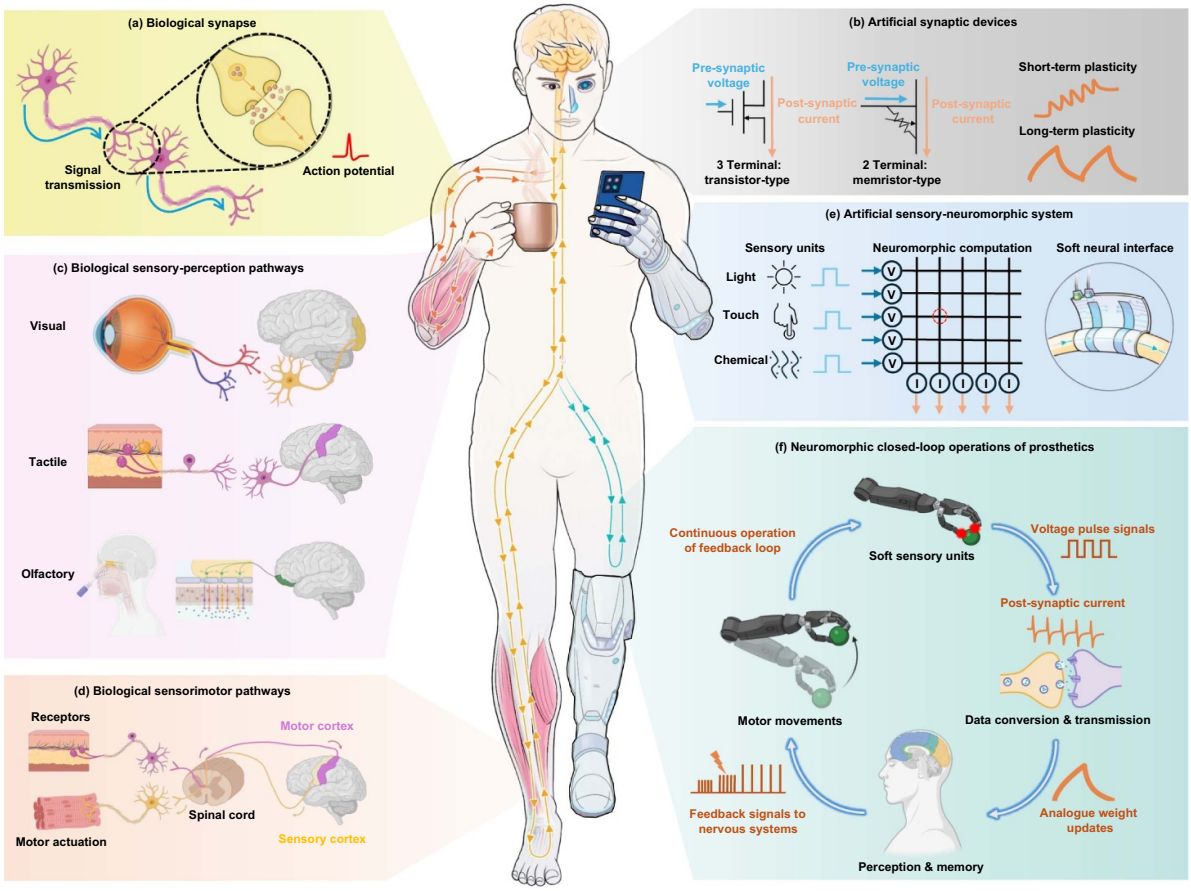

Figure 1. Overview of biological neural pathways (left) and an artificial prosthetic system (right) illustrating human-integrated closed-loop neuroprosthetic technologies. (a) Biological synapse. (b) Artificial synaptic devices. (c) Biologicalsensory-perception pathways. (d) Biological sensorimotor pathways. (e) Artificial sensory-neuromorphic system. (f) Neuromorphic closed-loop operations of prosthetics. [Illustrations in (a)–(f) Created in BioRender. Son, D. (2025) https://BioRender.com/f95i862].

with non-volatile properties[44−46]. Memristors and transistors are commonly used to fabricate artificial synapses, making them suitable for integration with sensors due to their physical, chemical, and electrical interactions within their inherent structures[47−51]. In addition to mimicking the structure and mechanisms of biological systems, recent research has focused on emulating neural pathways composed of trillions of neurons and synapses[52−55]. In biological systems, neural pathways include the afferent pathway, which transmits sensory signals from sensory receptors (e.g., skin, eyes, and nose) to the brain (Figure 1(c)), and the efferent pathway, which carries motor responses from the nervous system to muscles and other neural tissues (Figure 1(d)). These pathways form a sensorimotor loop, continuously updating commands and signals through feedback. Meanwhile, artificial sensory-neuromorphic systems, which replicate these partial loops or pathways, aim to create a fully connected closed-loop system for sensory perception by integrating synaptic devices with sensing units (Figure 1(e))[56−60]. Neuromorphic computing enabled by synaptic device arrays offers higher speed and reduced power consumption, while soft form factors facilitate signal transmission between damaged nerve tissues and prosthetic devices with minimal mechanical interference, paving the way for artificial sensory perception systems. Leveraging these advantages, demonstrating various pathways of the neural system through proper placement and connection of artificial sensors and synapses has become a key approach for developing customized prosthetic devices for daily use, offering efficient signal transmission and storage. Ultimately, by combining these bio-inspired sensory-perception-motor pathways, feedback signals followed by motor actuation enable the continuous closed-loop operation of neuroprosthetics, which is similar to that of the human body (Figure 1(f)).

In this review, we introduce the concept of a smart sensory-prosthetic system that integrates soft sensors with processing units and AI systems, along with the chip-level hardware implementation of neuromorphic computing devices for data processing. We also explore the mechanisms of synaptic devices with soft form factors that are highly compatible with irregular signals from soft sensors, as well as their applications in artificial sensory perception and the implementation of sensorimotor loops in clinical prosthetic systems and soft electronics. Finally, we propose a perspective that the combination of these enhanced components, pathways, and loops can lead to the development of a fully customized closed-loop electrical prosthetic system, offering sustained stability and convenience to individuals with physical impairments. Unlike other previous reviews and perspective papers, this

review not only provides the technical background and state-of-the-art advancements for each critical component of soft prosthetics—such as sensors, processors, synaptic devices, and integrated uni-/bidirectional artificial sensory systems—but also outlines future technical solutions and directions for achieving seamless and stable closed-loop prosthetics. We expect the following sections in this review to serve as a technical guide for next-generation human-machine interfaces and neuromorphic systems.

2. Developments of smart prosthetics and hardware-implemented in-memory computing devices

2.1. Smart prosthetics with soft sensors

For artificial perception, data acquisition and transmission are key factors for connecting real-world stimuli to prosthetic systems. The five biological senses—visual, auditory, olfactory, gustatory, and tactile—rely on numerous receptors to receive information from external stimuli in daily life[61,62]. Additionally, various signals such as electromyography (EMG), electrocardiography (ECG), electrocochleography (ECoG), and electroencephalography (EEG) are generated by biological tissues such as muscles, the heart, and the brain, which play important roles in healthcare diagnostics and capturing user intentions[63−66]. Despite significant advancements, challenges remain in achieving efficient and accurate physiological data acquisition, especially concerning signal interference and noise in dynamic and unexpected situations. To address these challenges, researchers are trying to integrate high-performance sensors with machine-learning-based smart AI technologies to enable precise recognition and control of prosthetic movements using obtained datasets[67−70]. Figure 2(a) presents a schematic of a prosthetic system under development, compatible with soft sensors. This system typically consists of sensing, processing, and actuating units, each optimized for higher accuracy, convenient usage, and biocompatibility. The following sections highlight the key trends and representative examples of research on sensor-integrated smart prosthetic systems.

2.1.1. Soft, bioadaptive prosthetics with sensory signal mapping. Biological sensors are crucial for prosthetic systems because they interpret physiological signals to enable accurate responses to user intentions and environmental changes. Early research primarily used rigid sensors, which had performance limitations due to various issues such as mechanical mismatch, poor conformal attachment, and inflammatory responses[75−77]. In contrast, softer sensors—designed with flexible and stretchable mechanical properties—offer significant advantages such as conformal adhesion to the irregular surfaces of human skin and durability against mechanical deformation caused by physical movement, enabling precise sensing even in noisy environments[78−80]. Various fabrication strategies have been developed to enhance the flexibility and stretchability of these sensors, such as adopting rigid island structures with wavy or buckled patterns and using strain-dissipative interconnections such as serpentine or kirigami-based designs[71,72,81,82].

Material innovations have also played a key role, with researchers combining conductive or semiconducting fillers with intrinsically stretchable elastomers[83−85] or depositing crack-based metals on elastomers[86,87]. By utilizing sensors with mechanical properties similar to human skin and eyes, these sensors can be effectively mapped to sense and control prosthetic or robotic movements through classification by microcontrollers. For example, in terms of visual sensors, a high-density curved image sensor array (CurvIS) based on a MoS_2-graphene heterostructure was proposed to mimic the structure of the biological eye[71]. This CurvIS, significantly thinner (51 nm) and capable of withstanding higher strain (∼23%) than silicon-based photodetectors (∼1%), was designed using a strain-isolation technique, with MoS_2 and graphene serving as photoabsorbing layers and interconnections, respectively (Figure 2(b)). The CurvIS array was conformally attached to a concave hemispherical dome, similar to the biological eye (Figure 2(c)). Finally, the proposed photodetectors not only captured images accurately without the need for additional IR filters but also amplified and programmed visual signals using microcontrollers and amplifiers, facilitating efficient electrical stimulation of the retina and ECoG signal measurements (Figures 2(d) and (e)). Meanwhile, artificial skin prostheses require multisensory capabilities, including responsiveness to various temperatures, motions, and tactile stimuli, along with mechanical softness. A representative example is the proposal of a stretchable prosthetic skin that incorporates ultrathin single-crystalline silicon nanoribbon (SiNR) sensor arrays for mechano- and thermosensation (Figure 2(f))[72]. This artificial skin features stacked structures composed of sensing layers (strain, pressure, temperature, and humidity sensors) and actuating layers (heaters) arranged using customized geometrical designs to maximize spatial efficiency and minimize interference between components. P-type doped SiNRs or gold nanoribbons are passivated with polyimide (PI) layers to create sensor devices with high piezoresistivity. To prevent mechanical failures due to low fracture toughness, the sensors and actuators were fabricated with ultrathin serpentine structures, which enhanced stretchability (∼20%). Integrating these devices into prosthetic limbs allowed for demonstrations of mapping changes in electrical properties (e.g., resistance, capacitance, and current) in response to various daily situations, further advancing the application of electronic skins (Figures 2(g) and (h)). Extensive research continues to focus on improving prosthetics with enhanced sensor performance and mechanical softness using various structural and material strategies.

2.1.2. Soft, bioadaptive prosthetic systems assisted by artificial intelligence. As sensor technology advances, the volume and diversity of biological signal data have increased, creating the need for effective processing, storage, and user-specific customization. To address these issues, AI methods, such as machine learning and cloud computing, have gained

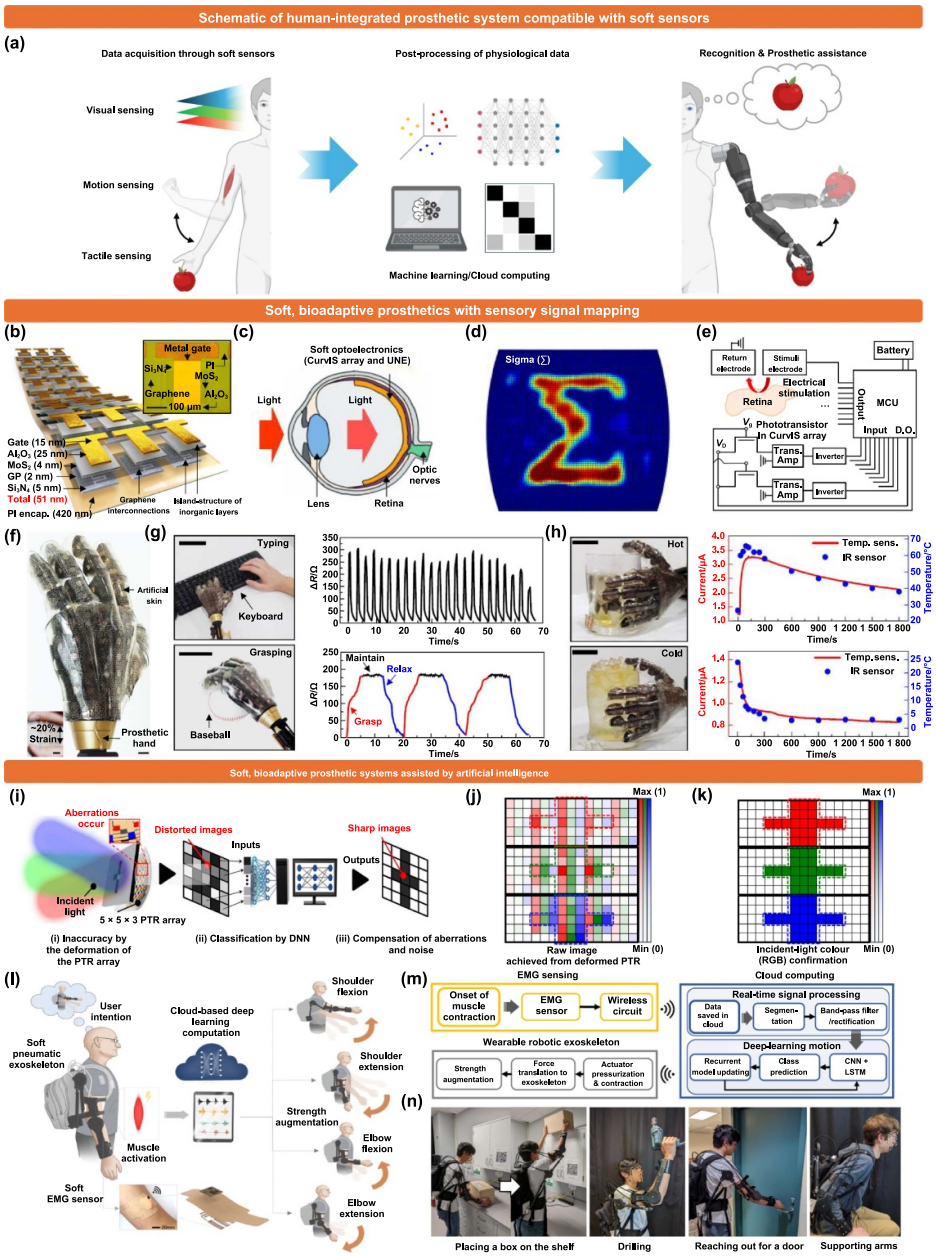

Figure 2. Prosthetic systems with soft sensors assisted by artificial intelligence. (a) Schematic of the human-integrated prosthetic system with soft sensors. (b)–(e) Human-eye-inspired flexible MoS_2-graphene image sensor array. (b) Schematic of the CurvIS array device. Inset: optical microscope image of a single MoS_2-graphene phototransistor. (c) Schematic of the ocular structure of the eye integrated with a soft optoelectronic device. (d) Image with a sigma shape captured by the CurvIS array. (e) Circuit diagram of electronics for detecting light signals (bottom) and applying stimulation to the brain (top). (b)–(e) Reproduced from[71]. CC BY 4.0. (f)–(h) Stretchable electronic skin with silicon nanoribbon. (f) Optical image of the artificial electronic skin with stretchable sensors and actuators on a prosthetic hand. Scale bar: 1 cm. Inset: photograph of 20%-stretched artificial skin. (g) Image of the prosthetic upper limb tapping a keyboard (top left) and corresponding resistance change of the SiNR pressure sensor (top right). Scale bar: 10 cm. Image of the prosthetic limb grasping a baseball (bottom left) with corresponding resistance change of the SiNR pressure sensor showing dynamics of the prosthetic hand in grasping, maintaining, and relaxing motions (bottom right). Scale bar: 5 cm. (h) Images of the prosthetic upper limb touching a cup of hot (top left) and cold water (bottom left), with corresponding current change in the SiNR temperature sensor (PIN diode, red), and the actual temperature trace measured by the IR sensor (blue dots) (hot: top right, cold: bottom right). Scale bar: 3 cm. (f)–(h) Adapted from[72], with permission from Springer Nature. (i)–(k) Stretchable quantum-dot nanocomposite-based phototransistor array devices to compensate for noise induced by mechanical deformation. (i) Schematic of visual prosthetic system improving accuracy of the mechanically deformed phototransistor array. (j) Normalized current signals of R, G, and B image patterns in mechanically deformed states. (k) Confirmation of the incident light color through a color-sensing algorithm based on corrected image patterns achieved after the application of the DNN from flat and deformed images. (i)–(k) Adapted from[73], with permission from Springer Nature. (l)–(n) Intelligent upper-limb exoskeleton for strength assistance and augmentation. (l) Overview of the operation of intelligent upper-limb prostheses with soft EMG sensors and actuators. (m) Flowchart describing the process of intent-driven exoskeleton actuation for strength augmentation. (n) Photograph of exoskeleton in daily use. (l)–(n) Reproduced from[74]. CC BY 4.0. [Illustrations in (a) Created in BioRender. Son, D. (2025) https://BioRender.com/s47x778.].

significant attention for their ability to handle large datasets with high accuracy and automated processes, and for integration with soft electronics[73,74,88–90]. The combination of AI technologies with soft electronics not only offers the ability to decouple signal variations and noise due to sensor deformation[74,88], but also to analyze user-specific signal characteristics, facilitating the development of customized prosthetics tailored to individual needs[73,89,90].

A notable example is the application of a deep neural network (DNN) algorithm with a 5 × 5 × 3 shape-tunable phototransistor array, which maintains performance even when deformed, mimicking the adaptability of the human eye[73]. Leveraging surface energy mismatch between materials, a semiconductor channel composed of poly[2.5-(2-octyl dodecyl)-3,6-diketopyrrolopyrrole-alt-5,5-(2,5-di(thien-2-yl)thieno[3,2-b]thiolphene)](PDPP2T-TT-OD) semiconductive materials and quantum dots (QDs) mixed with a polystyrene-block-poly(ethylene-ran-butylene)-block-polystyrene (SEBS) elastomer matrix was introduced as a stretchable photosensitive layer. Multispectral sensors are fabricated by stacking RGB pixels in a misaligned structure. Optical aberrations caused by deformation were corrected using machine learning, demonstrating the potential of this technology as a visual prosthesis (Figure 2(i)). Raw images obtained from the deformed device were corrected using a color-sensing algorithm based on a DNN algorithm and softmax function, yielding a high-accuracy visual information sensing system (Figures 2(j) and (k)).

In another study, an exoskeleton equipped with soft EMG sensors and cloud-computing processing methods was developed for customized prosthetics[74]. Soft EMG sensors composed of stretchable gold nanomembrane electrodes on a silbione substrate with serpentine designs, a silicon-based adhesive patch, a flexible circuit, and a switchable battery were conformally attached to the skin surface of various muscles to capture user intentions through muscle activation. Signals from the sensors were wirelessly transmitted to a cloud-computing server through a flexible circuit with band-pass filters and rectifiers and utilized to recognize muscle activation and predict motion classes in real time using deep learning techniques such as convolutional neural networks (CNN) and long short-term memory (LSTM) (Figure 2(m)). While the cloud-computing server stored muscle activation data for real-time applications, CNN and LSTM methods efficiently classified large data volumes, minimized variations between subjects, and ensured consistent performance. Pneumatic artificial muscles integrated with soft EMG sensors contract based on predicted classes, driving exoskeleton movements that augment the user's strength according to their intentions. This AI-driven prosthetic system demonstrated a maximum accuracy of 97.01%, enabling the successful use of prosthetics in daily life (Figure 2(n)). Thus, the integration of advanced sensor technologies with AI-driven data processing has significantly advanced the development of highly accurate, user-customized prosthetic systems.

2.2. Modern fully hardware-implemented neuromorphic computing system integrated with CMOS-compatible compute-in-memory chip

2.2.1. On-chip compute-in-memory system based on conventional memory devices. To realize a fully functional closed-loop neuroprosthetic system capable of replicating the sensorimotor functions of natural organs, it is essential to implement sensory-mimicking artificial perception systems that can generate motor plans and execute correct actuation in response to perceived stimuli. In addition to sensory-receptor-inspired sensor devices with high sensitivity and selectivity, developing processor units capable of deriving more complex perceptions by recalling past sensory stimuli is crucial for integration into intelligent computing systems. To achieve this, artificial intelligence systems must transcend the traditional von Neumann computing architecture by combining storage and computing operations with high efficiency and low power consumption, making them suitable for portable platforms, such as wearable or implantable schemes that can interface with the human body. One promising approach is the development of neuromorphic systems that employ a compute-in-memory (CIM) scheme, mimicking the crossbar structures and operating methods of the brain's biological neurons and synapses to perform both data storage and computation within a single device. This approach resolves the bottleneck between computation and data storage units, thus maximizing power consumption efficiency. Among fully hardware-implemented computing-in-memory neuromorphic systems, the most advanced technology relies on CMOS devices[91–99]. Neuromorphic CIM chips based on static random-access memory (SRAM), whose device configuration consists only of CMOS transistors, have already been manufactured by industry (e.g., TrueNorth chips from IBM and LoiHi chips from Intel)[100,101]. Compared to other commercial devices, including dynamic random-access memory (DRAM) and flash memory, SRAM is preferred as a unit device for in-memory computing neuromorphic systems due to its high data access speed, low latency, and low standby power. Recent advances in SRAM-based neuromorphic chips focus on improving the computational efficiency of neural network models and introducing customized SRAM configurations and neuron circuits for specific advancements[102–112]. One notable advancement in SRAM CIM chips is the development of an accelerator for spike neural networks (SNN)[113]. This system features a synapse storage module (SSM) using transposed 8-T SRAM cells to store synaptic weights and perform analog spike accumulation (Figure 3(a)). The proposed analog neuromorphic chip integrates an SRAM synapse array with peripheral driving circuits, incorporating an input-to-spike converter (I2SC) circuit designed with a counter and pulse generator, a digital neuron module (DNM) composed of digital arithmetic logic units (ALUs), a 4-bit counter, neuron registers, a weight update module (WUM) containing ALU-based weight calculators and an update design block, and programmable configurations, while excluding analog-to-digital converters (ADC) and digital multipliers (Figure 3(b)).

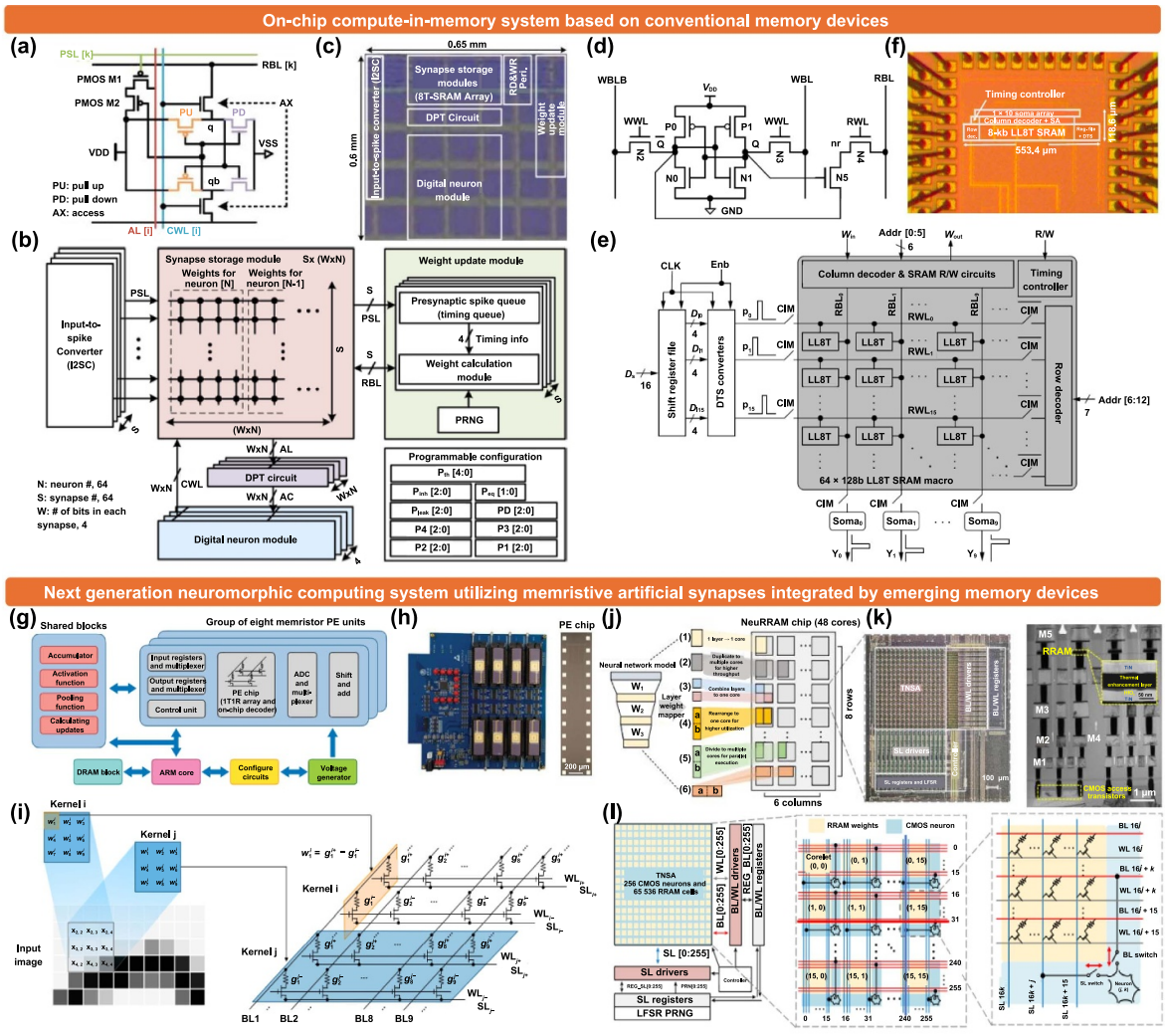

Figure 3. Fully hardware-implemented neuromorphic compute-in-memory systems integrating conventional CMOS memories or emerging memory devices into an artificial synapse array. (a)–(f) In-memory computing chips utilizing industry-level CMOS memory devices. (a) Transposed 8-transistor (8 T) SRAM cell for synaptic weight storage and analog spike accumulation. (b) Schematic of the overall system architecture of the compute-in-memory (CIM) chip with 8 T-SRAM synapses. (c) Microscopic image of the implemented CIM chip fabricated using 65-nm CMOS technology. (a)–(c) © (2020) IEEE. Reprinted, with permission, from[113]. (d) Schematic of the LL8T SRAM cell employed in ACIM operation. (e) Block diagram of the SNN-ACIM circuit using the LL8T SRAM array. (f) Microscopic image of a fabricated chip based on the 90-nm foundry process. (d)–(f) Reproduced with permission from[114]. CC BY-NC-ND 4.0. (g)–(l) Advanced neuromorphic systems employing memristive artificial synapses from next-generation resistive memory devices. (g) Schematic of the overall system architecture of a fully hardware-implemented memristive neuromorphic system incorporating eight memristor-based PE units, peripheral functional DRAM blocks, an ARM core, and control units. (h) Photograph of the PCB-implemented memristive neuromorphic hardware system. (i) Schematic of the memristor convolver circuit for convolution operations in a typical slipping process. $x_{m,n}$ indicates the relevant pixels at the crossing of rows m and n in a multiplexed artificial synapse array. Kernels i and j have synaptic weights of 3 × 3. All word lines (WL) were biased with $V_{WL} = 4.5$ V. The pulses applied to bit lines (BL) were 0.2 V, and the source lines (SL) were clamped with $V_{SL} = 0$ V during the entire parallel computation process. w represents the element value of the synaptic weight matrix, and g^+ and g^- represent the conductance values for the positive and negative weights in the differential pair, respectively. (g)–(i) Adapted from[115], with permission from Springer Nature. (j) Schematic of the overall system architecture of the multicore NeuRRAM chip and labeled maps of (1) to (6) neural-network layers onto the CIM cores. (k) Micrographic image of a single CIM core (left) and cross-sectional transmission electron microscopy (TEM) image illustrating the layer stack of the monolithically integrated RRAM and CMOS devices (right). (l) Block diagram of the NeuRRAM CIM core (left). The system incorporates a TNSA, driving circuits for BLs, WLs, and SLs, input-output (I/O) registers of the MVM, a LFSR, a PRNG, and a controller. The architecture of the TNSA consists of 16 × 16 cores with interleaving RRAM synaptic weights and CMOS neurons. Each neuron integrates inputs from 256 RRAM cells connected to the same horizontal BL or vertical SL (middle). Each corelet includes 16 × 16 RRAM arrays with one neuron connected to an individual BL and SL passing through the corelet. BL and SL function as both the input and output for the connected neuron (right). (j)–(l) Adapted from[116], with permission from Springer Nature.

The mixed-signal neuromorphic engine emulates 64 neurons and 16.4-K synapses, performing on-chip SNN learning through a timing-based stochastic spike-timing-dependent plasticity (STDP) model. The chip was manufactured using a 65-nm CMOS process, it achieves learning energy consumption below 200 nJ per image (148 nJ, 167 nJ, 194 nJ per image under 1.0 V, 1.1 V, 1.2 V input voltage respectively) and achieves modified National Institute of Standards and Technology (MNIST) accuracy above 70% (0.74, 0.79, 0.85 for input voltages of 1.0 V, 1.1 V, 1.2 V, respectively) with a total active area of the chip of 0.39 mm^2 (Figure 3(c)).

A more recent case for cutting-edge neuromorphic chip proposed an innovative integrated circuit (IC) design for SNN computations[114]. The system first implemented a pure analog compute-in-memory (ACIM) system capable of processing time-to-first-spike (TTFS) signals to realize a second-order leaky integrate-and-fire (SOLIF) SNN neuron model. A novel low-leakage 8-T (LL8T) SRAM structure was introduced to implement ACIM synapses (Figure 3(d)). The proposed SRAM synapse cell incorporates a conventional 6-T SRAM with a 2-NMOS cascode read port, differing from the standard 8-T SRAM by connecting to the source node at the read-port transistor, resulting in disturbance-free read operations with minimal current leakage. The overall system configuration of the SNN neuromorphic chip comprised a 64 $\times$ 128 LL8T-SRAM synapse array and peripheral circuitry with 16 $\times$ 4-bit shift registers, 16 DTS converters, and 10 soma circuits (Figure 3(e)). The fully integrated SOLIF analog neuromorphic chip manufactured using 90-nm CMOS technology performed the complete on-chip operation, including spike generation and inference, occupying an active area of 0.066 mm^2 (Figure 3(f)). The system implementing 10 neurons and 160 synapses demonstrated an average inference accuracy of 81.4% and an energy efficiency of 4.74 pJ per inference per neuron.

2.2.2. Next generation neuromorphic computing system utilizing memristive artificial synapses integrated with emerging memory devices. As discussed earlier, full hardware-implemented neuromorphic systems based on foundry-level memory devices offer high-density integration within a small area, on-chip learning, and inference with low-power operation, due to their high compatibility with advanced nanoscale CMOS technology. Despite these practical advances, existing CMOS-compatible neuromorphic systems using conventional high-speed memory represented by SRAM face limitations. Specifically, the large unit cell size restricts the integration density of synapse arrays, and the volatile storage nature of SRAM does not align with the long-term goals of neuromorphic computing.

In recent years, next-generation neuromorphic systems integrated with emerging unit devices have been established and intensively developed[117–122]. In particular, a memristor, whose conductance changes depending on an applied electrical field, is considered the component most similar to the operational mechanism of a biological synapse. Numerous efforts have been made to improve memristive devices and develop artificial synapses by integrating them. Emerging storage devices, which are versatile in several figures of merits including unit cell size, scalability, latency, endurance, and retention, are being explored to replicate the operational scheme of the memristor. Among these, resistive random-access memory (RRAM) is a promising candidate for memristive devices due to its resistive operation method. Data reading and writing occur within a switching layer between two-terminal electrodes, where the electrical resistance of the active layer changes with the input voltage. Significant progress has been rapidly made with neuromorphic compute-in-memristor systems exploiting RRAM-based artificial synapse arrays[123–132].

One of the significant breakthroughs was the development of the first fully hardware-implemented memristor chip[115]. The unit cell of the artificial synapse used a 1 transistor 1 RRAM (1T1R) memristor. RRAM, which comprises stacked thin films of TiN/TaO_x/HfO_x/TiN in the switching layer, provides reliable resistive operating performance. A single synaptic processing element (PE) unit for neuromorphic hardware was integrated with a 2 048 cell memristor array. The overall system architecture of the neuromorphic chip incorporates 8 memristor-based PE units and peripheral functional modules, including a DRAM block, an Acorn RISC Machine (ARM) core, control units, decoding circuitry, and a voltage generator (Figure 3(g)). This first fully hardware on-chip memristive neuromorphic system was integrated into a single PCB subsystem (Figure 3(h)). Utilizing artificial synapses based on multiplexed memristor arrays, the system successfully performed training and inference operations with a CNN model, executing parallel multiply-accumulate (MAC) computations. The system implemented parallel memristor convolvers and processed convolutional kernel weights using the ex-situ/*in-situ* hybrid training method, yielding improved accuracy in 2D images compared to conventional weight transfer methods (Figure 3(i)).

A more recent advancement in on-chip memristive neuromorphic hardware demonstrated a 48-core CIM chip with a total of 3 million RRAM cells, each consisting of 256 $\times$ 256 RRAM cells and 256 CMOS neuron circuits (Figure 3(j))[116]. The memristor unit cell for the artificial synapses adopted the 1T1R configuration. The multiplexed memristor matrix consisting of RRAM cells and CMOS neurons, referred to as a bidirectional transposable neurosynaptic array (TNSA), was designed to perform in-memory matrix-vector multiplication (MVM). The RRAM-CIM chip, named NeuRRAM, was integrated using a 130-nm foundry process, resulting in an active area of 159 mm^2 (Figure 3(k)). The total system architecture, containing the TNSA synaptic weight matrix, multiplexer, and driving circuits, registers, a linear-feedback shift register (LFSR) pseudo-random number generator (PRNG),

and a microcontroller unit, demonstrated the capability to execute diverse AI applications, flexibly using different neural network computation models with comparable software accuracy (Figure 3(l)).

3. Artificial synaptic devices with soft form factors

Recent advances in neuromorphic hardware computing chips using next-generation memory devices have shown significant progress. However, these studies have primarily focused on computations for recognizing and classifying large amounts of digital data using high-performance chips, which are unsuitable for reproducing human sensory functions. Additionally, when integrating these chips with soft sensor units designed to mimic human senses, there is a mechanical mismatch because the rigid form factor of the hardware is incompatible with the flexibility and stretchability required for the human body. These limitations highlight the need for soft synaptic devices. Soft synaptic devices not only address the mechanical mismatch, allowing for better integration with soft sensing units, but also provide a solution for creating systems capable of transferring, storing, and learning sensory signals.

To evaluate the performance of such synaptic devices, numerous universal parameters can be employed. For artificial synaptic devices, these parameters include electrical metrics such as the number of conductance states, nonlinearity, asymmetry, response time, dynamic range (on/off ratio), memory window, and energy efficiency. Additionally, stability and reliability metrics, such as retention time, endurance, and cycle-to-cycle variation, are critical for assessing robustness of fabricated artificial synapses. Specifically, for soft devices, it is particularly important that these characteristics are maintained even under mechanical deformation, ensuring consistent performance when integrated with flexible or stretchable systems. When applied within sensory-neuromorphic systems, the diversity of their configurations—tailored to emulate different human sensory modalities such as vision, touch, or hearing—makes direct quantitative comparisons challenging. However, the performance of such systems can be evaluated by achieving classification accuracy on given datasets (e.g., MNIST handwritten images, ECG arrhythmia datasets, etc.) trained using neural network software based on the synaptic parameters of synaptic hardware, offering a practical approach to assess their integrated performance. These metrics provide a foundation for meaningful comparisons and advancements in the area. The following section introduces various types of soft synaptic device structures and their operating mechanisms, highlighting their potential to overcome existing challenges and advance the field.

3.1. Soft artificial synaptic devices based on three-terminal transistors

Three-terminal (3T) transistor-based soft synaptic devices typically consist of a channel layer made from semiconducting materials, a gate dielectric layer, and source, drain, and gate electrodes. The gate electrodes and channel layer function as presynaptic and postsynaptic membranes, respectively. Signal transmission occurs through the channel layer, whereas the synaptic weights are independently modulated via the gate terminals. This separation of signal transmission and weight modulation makes 3T-based devices particularly well-suited for integration into larger systems, as it allows for more precise control and scalability. Detailed descriptions of structures and working mechanisms are provided in the following sections.

3.1.1. Floating gate transistor. A floating gate transistor (FGT) is a key structure used in NAND Flash memory, a well-established silicon technology for non-volatile data storage[133–139]. The structure of FGT-based synaptic devices is similar to that of conventional field-effect transistors but includes two gates. One is a control gate, which functions as a gate in standard transistors, and the other is a floating gate. The floating gate, insulated by both a tunnelling oxide layer and a gate dielectric layer, is located between the control gate and semiconductor channel (Figure 4(a)). When a voltage is applied to the control gate, electronic charges flowing between the source and drain are injected into the floating gate through the tunnelling oxide layer and accumulated on the floating gate. Once charges are injected, a higher gate voltage is required to maintain the same current level, leading to an increase in the threshold voltage (V_{th}). Conversely, when the charges are released, V_{th} returns to its initial value. This shift in V_{th} imparts memory capabilities, making FGT suitable for use in synaptic devices.

3.1.2. Ferroelectric field-effect transistor. Ferroelectric field-effect transistors (FeFET) employ ferroelectric materials[140–145] as gate dielectrics, allowing modulation of channel conduction by the electrical field through adjustment of the polarization state of the ferroelectric dielectrics (Figure 4(b)). When a gate voltage (electric field) is applied, the dipoles in the ferroelectric insulator gradually align, thereby accumulating carriers of opposite polarity to the dipoles at the interface between the semiconductor and ferroelectric insulator layer, which can modulate the conductivity of the channel. On the other hand, when an electric field is applied in the opposite direction, the dipoles in the ferroelectric insulator realign, redistributing the accumulated carriers at the semiconductor/ferroelectric interface. This reversal of polarization leads to the modulation of the channel conductivity in the opposite manner, either increasing or decreasing the channel current depending on the initial polarization state. This switching behavior enables FeFETs to function as non-volatile memory and makes them suitable for neuromorphic applications.

3.1.3. Electrolyte-gated transistor: electrical double layer transistor & electrochemical transistor. The configuration of an electrolyte-gated transistor is similar to a conventional field-effect transistor, with the key difference that the gate dielectric insulator is substituted with an electrolyte (either liquid or solid), resulting in larger gate capacitance and lower driving voltage[146–155]. When a gate voltage is

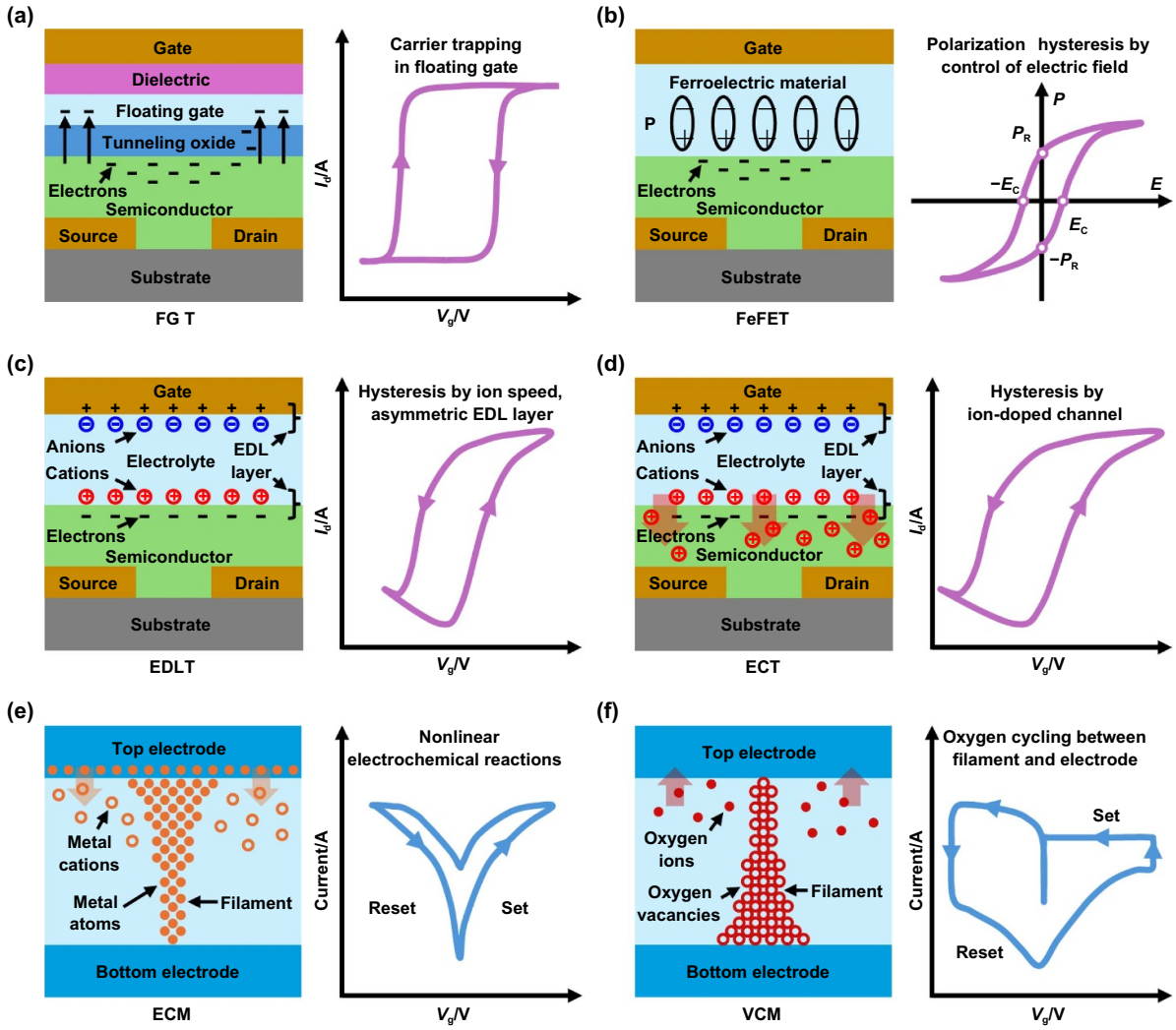

Figure 4. Schematic of various soft artificial synaptic devices and their representative electrical properties, including 3T devices: (a) floating gate transistor, (b) ferroelectric field-effect transistor, (c) electrical double-layer transistor, and (d) electrochemical transistor, and 2T devices: (e) electrochemical metallization memory and (f) valence change memory.

applied, the ions inside the electrolyte migrate to the channel layer, forming an electrical double layer (EDL) at the electrolyte/semiconductor interface. This structure is known as an electrical double-layer transistor (EDLT), as shown in Figure 4(c). Alternatively, ions may penetrate the bulk of the semiconductor, forming an electrochemical transistor (ECT), as shown in Figure 4(d). This modulates the channel conductance through electrostatic or electrochemical doping mechanisms. Once the gate voltage is removed, the current in the EDLT decays rapidly due to the quick spontaneous relaxation of the ions that have migrated only within the electrolyte. In contrast, the ECT current decays more slowly due to the long-lasting doping effect created by the redox reaction in the semiconductor. This results in a long-lasting doping effect and a relatively gradual decrease in the current. Owing to the aforementioned operation mechanism, electrolyte-gated transistor-based soft synaptic devices, such as EDLT and ECT, operate at lower voltage levels owing to their high coupling efficiency between the gate and channel, making them a promising option for neuromorphic applications.

3.1.4. Emerging material-engineered transistor. In addition to the transistor-based synaptic devices discussed above, recent research has actively explored various innovative material designs for synaptic devices. Notably, chargeable semiconductors, ambipolar semiconductors, and polymer electrets have emerged as promising candidates for next-generation synaptic devices. Chargeable semiconductors are materials designed to efficiently store and transport charge, simplifying the structure of transistor-based synaptic devices and making them crucial for applications in non-volatile memory and neuromorphic computing[156,157]. Their structures incorporate defects or molecular arrangements that serve as charge-trapping sites, where electrons or holes are captured in localized states, enabling precise conductance control and emulation of synaptic behaviors such as long-term potentiation and depression. Ambipolar semiconductors, capable of transporting both electrons and holes, enable bidirectional signal modulation (both n-type and p-type behaviors) within a single device. This dual functionality simplifies circuit design and facilitates multifunctionality with reconfigurable capabilities.

For synaptic applications, ambipolar semiconductors employ mechanisms similar to chargeable semiconductors, where trapped electrons or holes allow the implementation of bidirectional synaptic behavior. This enables excitatory and inhibitory signals to be processed within the same device, emulating complex synaptic plasticity in neuromorphic systems[158−160]. Polymer electrets, as dielectric materials, can temporarily capture electrons or holes to establish a quasi-permanent electric field. This occurs through a combination of physical charge trapping at defect sites, polarization of dipolar molecules within the electrets, and charge accumulation at the interfaces between metal and the electret. Therefore, even after the gate electrode voltage is removed, these materials retain changes in conductance, enabling bidirectional shifts in the threshold voltage. Their ability to maintain polarization over extended periods ensures reliable long-term synaptic weight states, even in dynamic environments, making them highly attractive for applications in artificial synaptic transistors[161,162].

3.2. Soft artificial synaptic devices based on two terminal memristors

Two-terminal (2T) memristor-based soft synaptic devices typically feature a metal-insulator-metal (MIM) structure, where an insulator between two electrodes implements a synaptic response by modulating the conductance between the electrodes. One electrode acts as the presynaptic terminal, receiving voltage pulses, whereas the other electrode acts as the postsynaptic terminal, delivering current. The simple structure and operating principle of 2T-based devices allow for easy fabrication of crossbar arrays, making them ideal for high-density electronic applications. Detailed descriptions of these devices categorized by their operating mechanisms are provided in the following sections.

3.2.1. Electrochemical metallization memory. Electrochemical metallization memory (ECM) operates by forming and dissolving conductive filaments (CFs) within an insulating matrix. This resistive switching process is initiated when an external electric field is applied to the device. When a positive bias is applied to the top electrode, typically made from an active metal like Ag or Cu, etc.[163−168], metal atoms oxidize into cations (e.g., Ag^{+} or Cu^{2+}) and migrate across the insulator towards the opposite bottom electrode. Upon reaching the bottom electrode, these metal cations are reduced and deposited as neutral metal atoms, forming conductive filaments between the electrodes that enable the transition of the device into a low-resistance state (LRS), known as the set process (Figure 4(e)). When a negative bias is applied, the metallic atoms forming the CFs reoxidize and diffuse away, dissolving the filament and returning the device to a high-resistance state (HRS), which is known as the reset process. This fast, reversible switching between LRS and HRS makes ECM-based artificial synapses strong candidates for neuromorphic computing applications.

3.2.2. Valence change memory. Valence change memory (VCM) usually employs inert metal electrodes such as Au or Pt to prevent ion migration from the electrodes. The migration of oxygen ions (O^{2-}) within the metal oxide insulating layer (e.g., TiO_2 or HfO_2) leads to the formation or elimination of oxygen vacancies, which create CFs and modulate the resistance of the oxide layer[169−173]. During the set process, as shown in Figure 4(f), a positive bias drives the oxygen ions away from the anode (bottom electrode) toward the cathode (top electrode). This migration causes oxygen vacancies to accumulate near the anode, forming a localized conductive filament, and transitioning the device into an LRS. Alternatively, during the reset process, applying a reverse bias causes oxygen ions to migrate back to the anode, filling the vacancies and breaking the conductive path, thereby restoring the device to an HRS. VCM-based artificial synapses offer significant advantages for neuromorphic systems due to their multilevel resistance, scalability, and ability to emulate synaptic behaviors.

4. Biological & artificial sensory-neuromorphic systems

4.1. Visual sensory-neuromorphic systems with artificial synaptic devices

Approximately 80% of external environmental information is processed through vision, making it essential to replicate biological visual systems in developing human-like robotic systems[174,175]. In biological visual perception, as illustrated in Figure 5(a), rod and cone photoreceptor cells in the eye detect various wavelengths and light intensities, transmitting the signals to the brain through bipolar and ganglion cells passing through multiple synapses. To emulate this process, artificial visual perception systems have been developed using synaptic devices that enable high-performance, low-power recognition, memorization, learning, and actuation[176−180]. Programmable synaptic devices, which use both electronic and optical signals as inputs have been extensively studied[181−184]. In addition, optoelectronic synaptic circuits that combine photosensitive elements with electronic synaptic devices have been proposed[185−187]. These synaptic devices, including two-terminal (e.g., memristors) and three-terminal devices (e.g., Organic electrochemical transistors (OECTs), FeFETs, and photosensitive thin-film transistors), have been fabricated with flexible, stretchable soft form factors, allowing for closer mechanical and functional replication of biological visual sensory organs[188−193]. The following section introduces the research efforts focused on mimicking the various functions of the human eye using artificial synaptic devices.

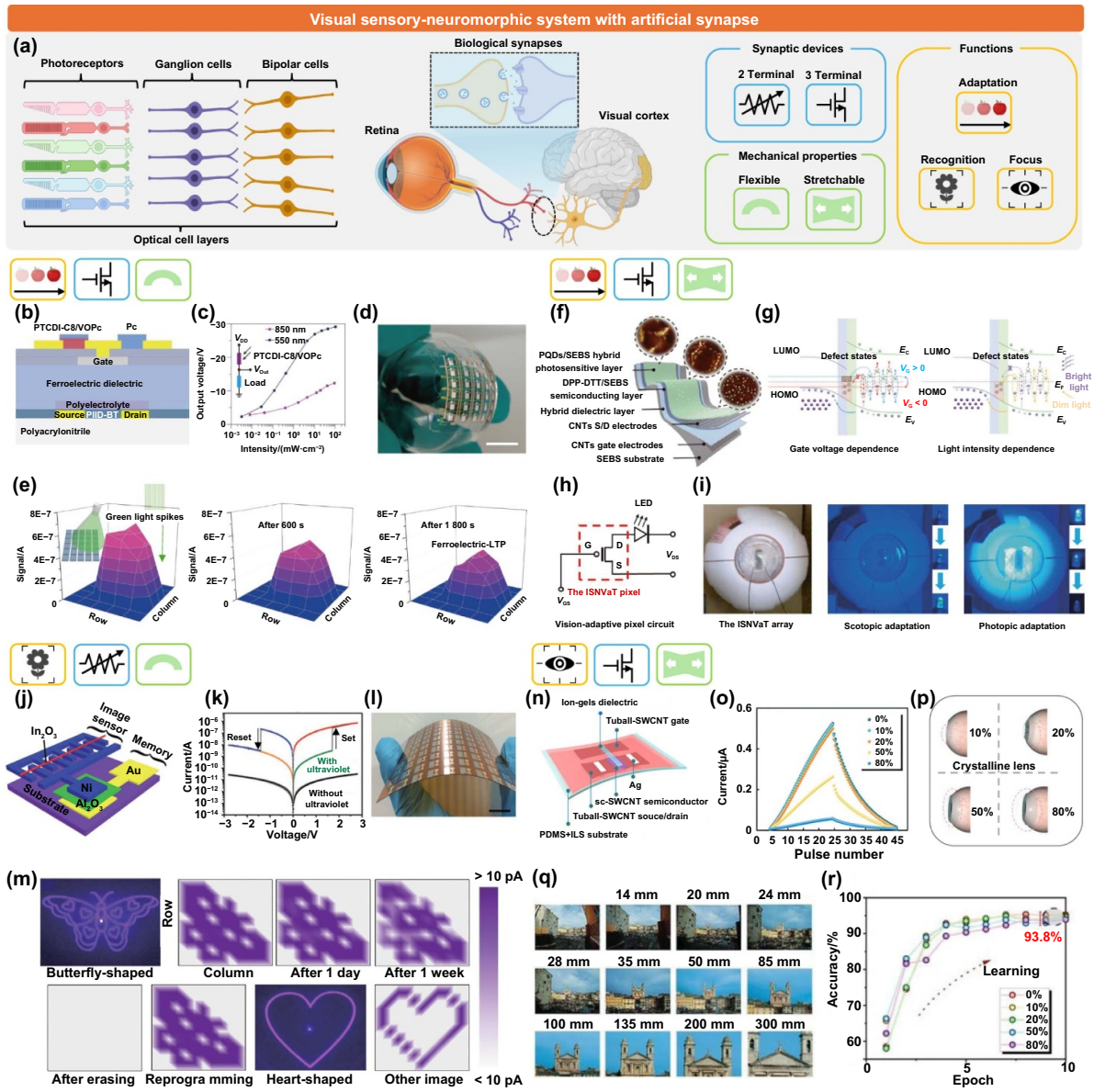

Figure 5. Soft visual sensory-neuromorphic system with artificial synaptic devices. (a) Schematic of biological visual sensory perception pathways where external visual stimuli are transmitted from optical receptor cells to the visual cortex via synapses. (b)–(e) Ultra-flexible LOND for an artificial visual perception system. (b) Illustration of the cross-sectional structure of LOND. (c) Output characteristics correspond to the voltage divider circuit under light at wavelengths of 850 and 550 nm. (d) Photograph of a LOND array conformally attached to a hemisphere. Scale bar: 7.5 mm. (e) Signals in the LOND array recorded after incident green light exposure (10.80 mW·cm^{-2}, 64 Hz for 4 s, left), remaining signals in the LOND array after 600 s (middle) and 1 800 s (right) retention. (b)–(e)[189] John Wiley & Sons. © 2018 WILEY-VCH Verlag GmbH & Co. KGaA, Weinheim. (f)–(i) Intrinsically stretchable neuromorphic transistors with stable vision-adaptive properties under biaxial stretching. (f) Schematic of the structure of elastic heterojunction-based ISNVaT. (g) Operating mechanism of vision-adaptation properties with variations in gate voltage (left) and light intensity applied to ISNVaTs. (h) Circuit schematic of an ISNVaT pixel serving as an LED driver. (i) Photograph of the ISNVaT pixel attached to an ocular prosthesis (left), showing scotopic (middle), and photopic adaptation (right) of the ISNVaT pixel, turning the LED from dark to bright, and vice versa. (f)–(i) Reproduced from[188]. CC BY 4.0. (j)–(m) Flexible memristor devices operating under UV light for visual memory systems. (j) Schematic illustration of the bioinspired visual memory circuit integrated with an image sensor and resistive switching memory device. (k) I–V characteristics of the bioinspired visual memory circuit under UV light illumination. (l) Photograph of the integrated device arrays on flexible polyimide substrates. Scale bar: 1 cm. (m) Visual image storage and reusability of flexible visual memory device arrays for light signals of various shapes. (j)–(m)[190] John Wiley & Sons. © 2018 WILEY-VCH Verlag GmbH & Co. KGaA, Weinheim. (n)–(r) Stretchable neuromorphic vision system with focal adjustment properties using carbon nanotube optoelectronic synaptic transistor arrays. (n) Schematics of SSOSTFTs. (o) LTP/LTD curves with successive UV light and voltage pulses under 0–80% stretching strain. (p) Simulated crystalline lens bending from stretching force. (q) Photographs showing the relationship between focal length and pupil area corresponding to lens stretching. (r) Enhanced ozone prediction increased with the number of training epochs in the neural network using the simulated weight update rule of SSOSTFTs under various strain conditions. (n)–(r)[191] John Wiley & Sons. © 2023 Wiley-VCH GmbH. [Illustrations in (a) Created in BioRender. Son, D. (2025) https://BioRender.com/l01d460.].

4.1.1. Scotopic & photopic adaptation. In biological visual system, the ability to adapt to varying light intensity levels in the environment—scotopic or photopic adaptation—enables object recognition under both dim and bright conditions. Research into artificial photonic synapses has demonstrated similar time-varying adaptation through mechanisms of charge trapping induced by light signals and subsequent detrapping over time[188,189,194]. As previously discussed, integrating photosensitive elements and photo-insensitive electrical synaptic devices has garnered significant attention for efficient conductance modulation and enhanced visual information processing speed. Representatively, an ultra-flexible light-triggered organic neuromorphic device (LOND) was presented using a ferroelectric/electrochemically modulated organic synapse with a photovoltaic divider composed of a photosensor and a load resistor[189] (Figure 5(b)). Under varying light conditions, the conductance of the photosensor changed, modulating the output voltage of the photovoltaic divider circuit, which was then transmitted to the gate terminal of the electrical organic synapse for programming (Figure 5(c)). To emulate retinal function, the LOND array was conformally adhered to a hemispheric surface, exhibiting soft mechanical characteristics (Figure 5(d)). The device demonstrated the ability to receive light signals and retain memory, mimicking scotopic adaptive functions after exposure to strong green light (Figure 5(e)).

However, challenges such as spatial inefficiency, data processing latency, and limited stretchability remain in sensor-synapse circuitry integration. To address these issues, an intrinsically stretchable neuromorphic vision-adaptive transistor (ISNVaT) was recently introduced[188]. This single-transistor device exhibited superior photoadaptation and neuromorphic performance, surpassing the biological visual system in speed and power efficiency, utilizing a heterojunction between the photosensitive and semiconducting layers (Figure 5(f)). The photosensitive layer, featuring quasi-continuous microsphere morphologies, was fabricated by adjusting the ratio of the perovskite QDs to the SEBS elastomer, forming thin films on a polydimethylsiloxane (PDMS) substrate, with surface energy tuned through O_2 plasma treatment. The photoadaptive mechanisms were investigated using various electrical and optical stimuli, as shown in Figure 5(g). A positive (negative) gate voltage enhanced (reduced) the recombination of holes and excitons, which were immediately generated by light illumination for erasing properties (Figure 5(g), left). The intrinsic trap states due to the heterojunction structure limited charge transport, leading to current saturation and demonstrating successful photoadaptation (Figure 5(g), right). Scotopic and photopic behaviors were demonstrated by conformally attaching the ISNVaT pixel device to an ocular prosthesis as an LED driver, demonstrating the biaxial stretchability and in-sensor computing capabilities of the device for next-generation visual prosthetics (Figures 5(h) and (i)).

4.1.2. Image recognition. Photonic synapses with optical neuromorphic modulation and computational properties effectively mimic cognitive tasks and biological visual systems with high accuracy and low power consumption. Leveraging the high performance of visual synaptic devices, these devices have recently advanced their applications in image recognition, including tasks such as color differentiation[187,195,196] and complex image pattern recognition[177,179,182,186,190,192]. The demonstrations typically involve either applying synaptic parameters extracted during the process of analog weight (conductance) changes to artificial neural networks or activating the device to meet decision-making conditions. A notable development is an artificial flexible visual memory device composed of In_2O_3-based UV-sensitive image sensors and Al_2O_3-based memristors[190]. The interdigitated electrode structures and regulation of the number of semiconductors micrometer-sized wires facilitated resistance-state matching by adjusting photocurrent levels (Figure 5(j)). As the resistance within the image sensor decreased, the increase in voltage across the memristor unit triggered a resistance-state transition from the OFF state to the ON state, thereby encoding light information into the memory device. In the absence of light, the stored information remains in the memory device until a reset voltage is applied (Figure 5(k)). The visual memory device array with scalable fabrication on a flexible PI substrate displayed visual memory characteristics corresponding to various UV light images over the long term (Figures 5(l) and (m)).

4.1.3. Focus adjustment. In biological visual systems, focus adjustment is achieved through dynamic changes in the curvature of the eye lens, allowing clear vision at varying distances[191,197,198]. Similarly, in artificial systems, synaptic properties modulated by optical and electrical stimuli enable precise vision adaptation to corresponding curvature angles. These innovations have significant potential for enhancing the precision and functionality of vision systems in human-like robotics. Recently, stretchable optoelectronic synaptic thin-film transistors (TFTs) incorporating semiconducting single-walled carbon nanotubes (sc-SWCNTs) and CdSe/ZnS quantum dots (QDs) as active layers have been reported[191]. The stretchability of the device was enhanced by using an ionic liquid (IL)-PDMS composite substrate and an ion gel dielectric with $[EMIM]^+[TFSI]^-$ (1-ethyl-3-methylimidazolium bis (trifluoromethanesulfonyl) imide) (Figure 5(n)). This mechanical softness allows modulation of focal distances under various strain conditions, similar to the crystalline lens of the human eye, as demonstrated through long-term potentiation and depression (LTP/LTD) curves under dynamic conditions (Figures 5(o) and (p)). Focus adaptation, closely related to pupil area, which regulates the amount of light entering the eye, was mapped with diverse bending and stretching conditions of artificial visual devices, demonstrating high accuracy in sensing and learning abilities (Figures 5(q) and (r)). These advancements in neuromorphic visual applications, mimicking biological eye functions in soft-form factors using innovative materials, device structures, and circuits, have paved the way for user-customized and reliable next-generation visual prosthetics.

4.2. Tactile sensory-neuromorphic systems with artificial synaptic devices

Tactile perception enables interactions with the environment by providing information about the size, texture, and shape of objects, allowing safe grasping, manipulation, and movement[199,200]. As shown in Figure 6(a), human tactile perception relies on various mechanoreceptors located in the epidermis, dermis, and subcutaneous tissues, such as Merkel cells, Meissner's corpuscles, Pacinian corpuscles, and Ruffini endings, which detect sensations such as touch, pressure, vibration, and texture. These external mechanical stimuli are converted into electrical signals that are transmitted through synapses to the somatosensory cortex, where information is processed and interpreted. In recent years, significant efforts have been made to develop systems that emulate human tactile perception for applications in robotics, prosthetics, human-machine interfaces, and other fields. Various tactile sensors employing capacitive[173,201,202], piezoelectric[203–205], piezoresistive[206–209], triboelectric[210–212], and ferroelectric mechanisms[213,214] have been actively researched. The following section introduces tactile sensory-neuromorphic systems that integrate various tactile sensors with artificial synaptic devices to construct artificial neural systems capable of performing advanced functions, such as mechanoreception emulation, afferent nerve signal transmission, and cognitive processing.

4.2.1. Mechanoreception emulation. Human mechanoreceptors are classified into two categories based on their response speed to mechanical stimuli and their adaptation to continuous stimulation: slow-adaptive (SA) mechanoreceptors (SA type I: Merkel cells and SA type II: Ruffini endings) and fast-adaptive (FA) mechanoreceptors (FA type I: Meissner's corpuscles and FA type II: Pacinian corpuscles)[218,219]. SA mechanoreceptors provide feedback for steady mechanical stimuli, such as sustained touch, pressure, or stretch, due to their slow or minimal adaptation to continuous input. In contrast, FA mechanoreceptors respond quickly to changes in mechanical stimuli, such as sudden touch, pressure, or vibration, enabling the nervous system to concentrate on detecting new stimuli. Developing artificial mechanoreceptors that emulate both SA and FA mechanoreceptors is crucial for replicating human tactile perception. As shown in Figure 6(b), a bioinspired flexible artificial system combining SA and FA mechanoreceptors with synaptic functionality has been proposed[215]. FA mechanoreceptors, based on a pressure sensor using the piezoelectric material poly(vinylidene fluoride-co-trifluoroethylene) (P(VDF-TrFE)), respond only to initial contact and the release of compression. SA mechanoreceptors, using the same device structure as the FA mechanoreceptors but incorporating a piezoelectric ionogel of P(VDF-TrFE) and the ionic liquid $[EMIM]^+[TFSI]^-$, produce a sustained voltage output under static pressure. Additionally, to mimic the synaptic plasticity of biological synapses, an EDLT-based synaptic device was fabricated on a flexible PI substrate using an ionogel of $[EMIM]^+[TFSI]^-$, polyurethane (PU) as the gate electrolyte dielectric, reduced graphene oxide (rGO) as the channel, and Au as the source-drain and gate electrodes. To demonstrate synaptic functionality, artificial SA and FA mechanoreceptors were integrated with an EDLT-based synaptic device, and compressive pressure with varying frequencies, amplitudes, durations, and numbers of touches were applied. As shown in Figures 6(c) and (d), the SA mechanoreceptor can sense and memorize tactile information through its synaptic properties. In contrast, the FA mechanoreceptor can only sense tactile information. The memory function of the FA mechanoreceptor was achieved by connecting a single rectifying diode between the FA mechanoreceptor and an EDLT-based synaptic device to convert the generated output voltage into a unidirectional potential.

4.2.2. Afferent nerve signal transmission. In biological tactile sensory systems, tactile information—also known as spiking neural activity or action potentials—is transmitted to the somatosensory cortex via spike-based communication. These spike signals allow for the quick and efficient transmission of information over long distances in the nervous system, being triggered only when sufficient input is received, making the system energy-efficient. Numerous studies have attempted to mimic efficient biological tactile sensory systems[220]. For instance, a ring oscillator-based bioinspired flexible artificial afferent nerve has been developed and connected to a pyramid-structured resistive pressure sensor functioning as an artificial mechanoreceptor and an ion-gel-gated synaptic transistor, as shown in Figure 6(e)[216]. Similar to biological SA-I afferent nerves, the organic ring oscillator generates action potentials with variable frequencies (0–100 Hz) based on data collected from clusters of resistive pressure sensors. These action potentials are integrated and converted into postsynaptic currents using an ion-gel-gated synaptic transistor. As pressure intensity increases, both the frequency and amplitude of the action potentials increase. While pressure duration does not change the frequency or amplitude of the action potentials, it can extend the duration of the signal applied to the ion-gel-gated synaptic transistor, leading to increased anion accumulation at the semiconductor-electrolyte interface and an increase in the postsynaptic current. As shown in Figure 6(f), this artificial afferent nerve can detect the direction and speed of moving objects and recognize Braille characters by integrating spatial and temporal tactile information from multiple sensors. When the object moves in the direction indicated by the red arrow, the postsynaptic current output from the ion-gel-gated synaptic transistor produces two spike clusters as the object passes over two pressure sensors over time (Figure 6(g)). By contrast, when the object moves in the direction of the blue arrow, it simultaneously passes over both sensors, forming a single large spike cluster (Figure 6(h)).

4.2.3. Pattern recognition. In the previous section, the process by which mechanoreceptors convert external mechanical stimuli into electrical signals in tactile sensory-neuromorphic systems was discussed, along with the role of afferent nerves

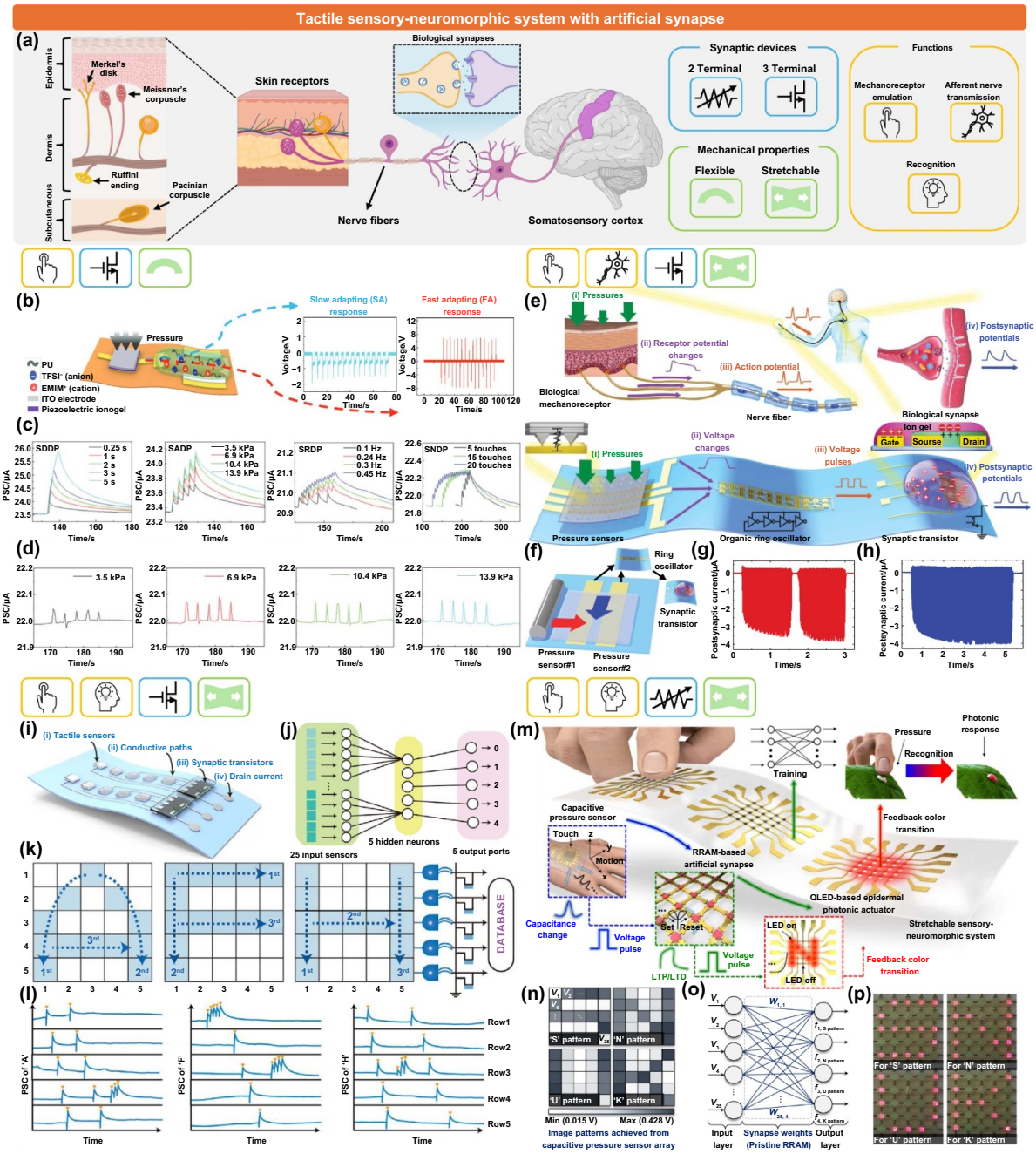

Figure 6. Soft tactile sensory-neuromorphic system with artificial synaptic devices. (a) Schematic of biological tactile sensory-perception pathways transmitting external stimuli from the mechanoreceptor to the somatosensory cortex via synapses. (b)–(d) Bioinspired flexible artificial system combining SA and FA mechanoreceptors with EDLT synapses. (b) Schematic of the bio-inspired artificial FA and SA mechanoreceptors and output characterization of SA and FA pressure sensors. (c) PSC of the SA mechanoreceptor regulating duration, amplitude, frequency, and number of pulses. (d) PSC of the FA mechanoreceptor by regulating pulse amplitude. (b)–(d)[215] John Wiley & Sons. © 2023 Wiley-VCH GmbH. (e)–(h) Stretched artificial afferent nerves for efficient signal transmission. (e) Schematic of a biological afferent nerve, including mechanoreceptors, nerve fibers, biological synapses, and artificial afferent nerves composed of pressure sensors, an organic ring oscillator, and a synaptic transistor. (f) Artificial afferent nerve with two pressure sensors detecting moving objects (red and blue arrows). PSC when the object moves in the (g) and (h) directions of the red and blue arrows, respectively. (e)–(h) From[216]. Reprinted with permission from AAAS. (i)–(l) Stretchable skin-conformable neuromorphic tactile system consisting of TENG sensors and ECT synapses. (i) Schematic of the integrated system with TENG tactile sensors and ECT synapses. (j) Schematic of handwritten letter processing (k) Demonstration of the writing paths for letters "A," "F," and "H." (l) Five PSC signals obtained from handwritten "A," "F," and "H" in the TENG tactile array. (i)–(l) Reproduced from[217]. CC BY 4.0. (m)–(p) Bioinspired SSNS for tactile pattern classification. (m) Schematic illustration of a bioinspired SSNS integrating a capacitive pressure sensor, 2 T VCM-based RRAM synapse, and QLED-based epidermal photonic actuator. (n) Input image patterns ("S," "N," "U," and "K") obtained by the artificial mechanoreceptors. (o) The ANN consisted of 25 input neurons corresponding to each artificial mechanoreceptor, four output neurons corresponding to each pattern, and 25 × 4 synapses connected to the neurons. (p) Photographs of the epidermal photonic actuator array visualizing the trained/inferred patterns of "S," "N," "U," and "K." (m)–(p).[173] John Wiley & Sons. © 2021 Wiley-VCH GmbH. [Illustrations in (a) Created in BioRender. Son, D. (2025) https://BioRender.com/h48b975.].

in transmitting these signals. Additionally, there has been active research on how the brain processes and interprets electrical signals transmitted via afferent nerves. One notable development involves a stretchable skin-conformable neuromorphic tactile system that integrates triboelectric nanogenerators (TENG) as tactile sensors and hydrogel-gated OECT synapses (Figure 6(i))[217]. The TENG device was fabricated using a stretchable PDMS substrate, with PDMS films at curing ratios of 10:1 and 20:1 serving as friction layers, and liquid metal eutectic gallium–indium (EGaIn) as the electrode. TENGs function as artificial mechanoreceptors that detect pressure and convert mechanical stimuli into electrical signals. The TENG device exhibits high sensitivity (∼0.04 kPa) and a broad pressure detection range (0.24–23.56 kPa, covering the human pressure perception range), with excellent stretchability (up to 100% strain). The OECT synapse, which uses Poly(3,4-ethylenedioxythiophene) polystyrene sulfonate (PEDOT:PSS) as the active channel, and soft PAAMPSA is introduced to enhance its stretchability. Additionally, NaCl hydrogel electrolytes were designed to achieve a balance of high-water content, low volatility, and high conductivity, with EGaIn electrodes used, similar to the TENG. The OECT synapses process signals by mimicking the memory and computing capabilities of biological synapses.

With both short- and long-term synaptic plasticity essential for learning and adaptive responses, the system encodes and recognizes tactile information, such as detecting movement direction and recognizing patterns such as Morse codes and handwritten letters. As shown in Figures 6(j), a 5 × 5 array of TENG sensors serves as the tactile input, and five synapse transistors function as hidden neurons to process information. Instead of extracting 25-dimensional information from the TENG array, the system extracts five postsynaptic current signals from the OECTs. When a touch is detected in any row of tactile sensors, postsynaptic current signals are generated in the corresponding transistor. For instance, when the letters "A," "F," and "H" are written in specific paths (Figure 6(k)), the system produces corresponding five postsynaptic current signals (Figure 6(l)). These letter directories of the codes are formed using peak-timing convolution encoding, facilitating the recognition and learning of handwritten inputs.

In another example, as shown in Figures 6(m), a bioinspired stretchable sensory-neuromorphic system (SSNS) was developed by integrating a capacitive pressure sensor, a 2 T VCM-based RRAM artificial synaptic device, and an epidermal photonic actuator made of a quantum dot light-emitting diode (QLED)[173]. This system incorporated a rigid island structure interconnected by a sinter-free printable conducting nanocomposite composed of Ag flakes and a self-healing polymer (PDMS-$MPU_{0.4}$-$IU_{0.6}$)[221,222]. The capacitive pressure sensor responded to strain-induced deformation when stretched (≈0.002 51 mm^{-1} at 60% strain) or pressed (≈0.594 kPa^{-1} at 0.9 kPa), due to its linear response to changes in capacitance with applied strain. To emulate synaptic functionality in skin-like systems, RRAM with an Al/TiO_2/Al layered structure was used as a neuromorphic device with cognitive processing abilities. The RRAM cells were fabricated on a wafer and transfer-printed onto a stretchable substrate, with each island bridged by intrinsically stretchable printed interconnects. The SSNS processes patterned stimuli through artificial mechanoreceptors based on capacitive pressure sensors (Figure 6(n)) and transmits voltage signals to an artificial neural network (ANN) (Figure 6(o)). After training the neural network with the patterned stimuli, the inferred signals were transmitted to the epidermal photonic actuator, which emitted light patterns matching the stimuli (Figure 6(p)). This integration of sensory detection, neural processing, and visual feedback highlights the potential of such systems for advanced applications such as wearable electronics and intelligent prosthetics.

4.3. Olfactory sensory-neuromorphic systems with artificial synaptic devices

The olfactory system plays a critical role in perceiving and distinguishing different odors, which are essential for activities such as appetite stimulation and food seeking, vital for survival. Additionally, it enables the recognition and avoidance of hazardous substances or environments while triggering appropriate emotional responses and behaviors based on perceived odors. Olfactory perception is initiated by the generation of electrical potentials resulting from the binding of scent molecules to olfactory receptors distributed along the nasal epithelium. These spikes pass through the amygdala and hippocampus and are finally transmitted to the olfactory cortex for processing, leading to odor awareness (Figure 7(a)). Inspired by biological olfactory systems, extensive efforts have been made to develop highly functional chemical sensor devices capable of detecting scent molecules and reacting rapidly to target materials. However, traditional gas sensors, despite their high sensitivity and selectivity lack the ability to store memories of gas stimuli—an essential feature for chemical information processing[223−233]. Therefore, the development of artificial olfactory synaptic devices capable of both chemical processing and sensing is critical for implementing neuromorphic systems that mimic this sensory scheme[234−239]. Artificial olfactory synapses have been typically designed as three-terminal devices employing a chemical-responsive channel material to facilitate chemical and electrical interactions, particularly in flexible devices[240]. The following section highlights examples of soft artificial olfactory synapses that emulate the functionality of the human nose using electrochemical devices.

The critical device configuration strategy for OECT-based artificial olfactory synapses is based on the utilization of chemically sensitive electrolytes that interact with the electrochemical channel via ion transportation triggered by an external chemical stimulus. In the first example, a soft artificial olfactory synapse developed using an OECT device was fabricated on a thin PI substrate with deposited gold (Au) electrodes. A

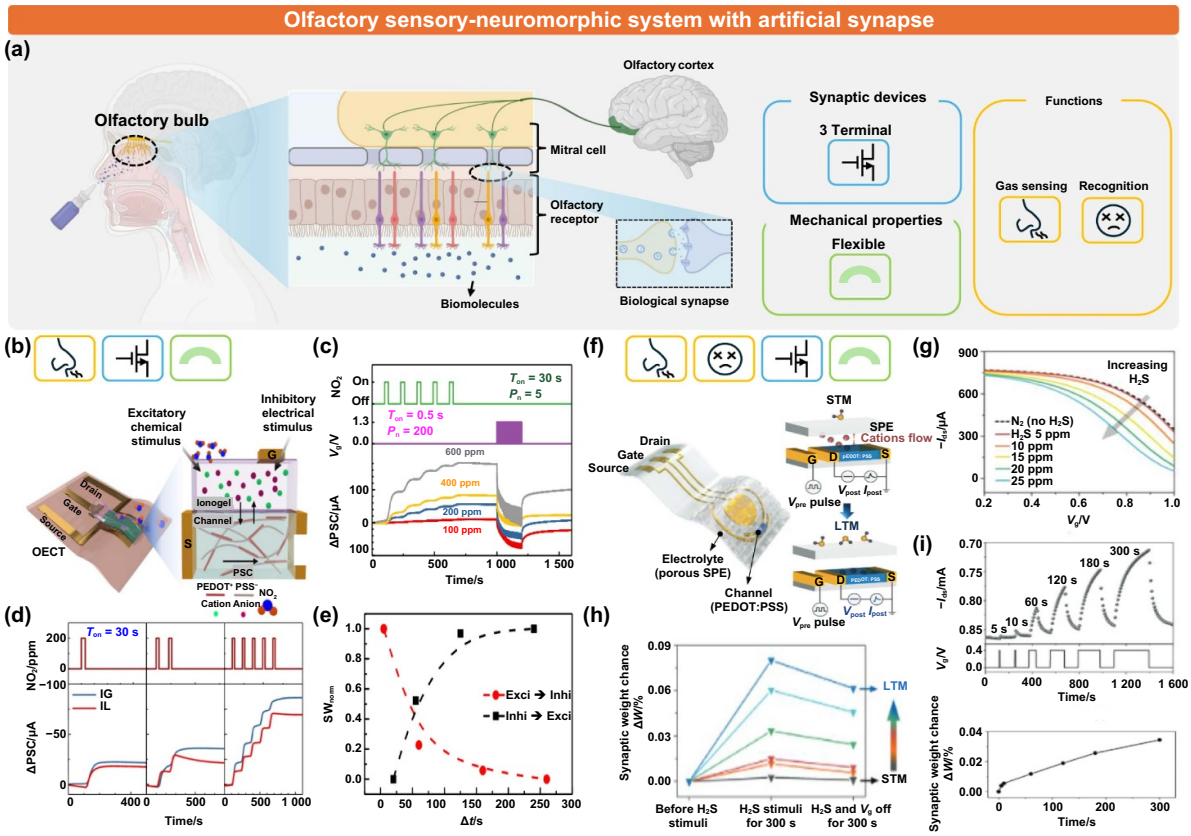

Figure 7. Soft olfactory neuromorphic system with artificial synaptic devices. (a) Schematic of the olfactory sensory system. The chemical stimuli applied by odorants are converted to electrical potential at the olfactory receptor neuron and transmitted to the olfactory cortex via synapses. (b)–(i) Bio-inspired flexible artificial system with soft olfactory receptors and synapses integrated with OECT. (b) Illustration of a flexible OECT-based synaptic device whose active domain consists of a PEDOT: PSS channel and a chemically responsive ionogel gate electrolyte (left). A cross-sectional view of the device illustrates the operating mechanism of the chemical receptor and synapse mimicking olfactory perception (right). (c) Changes in post-synaptic current (ΔPSC) of the flexible artificial olfactory synapse controlled by the concentration of NO_2 and gate modulation. (d) Time-dependent profile of ΔPSC with different numbers of NO_2 pulses at a concentration of 200 $\mu L \cdot L^{-1}$. (e) Normalized synaptic weight as a function of the time interval between excitatory and inhibitory stimuli (black: inhibitory to excitatory stimuli; red: excitatory to inhibitory stimuli). (b)–(e) Reproduced from[241]. CC BY 4.0.(f) Illustration of a flexible OECT-based synaptic device with a PEDOT: PSS channel and a porous SPE film fabricated by the breath-figure method (left), and a cross-sectional view showing the operating mechanism for the transition from STM to LTM, imitating gasotransmitter-mediated plasticity for gas sensation and hazard recognition (right). (g) Differences in the output current of the OECT artificial synapse distinguishing the concentration of H_2S gas at 5 $\mu L \cdot L^{-1}$. (h) Normalized synaptic weight driven by H_2S stimuli at different concentrations, showing the STM-to-LTM transition. (i) Output current response modulated by different input pulses, with the corresponding normalized synaptic weight change as a function of time exhibiting the gasotransmitter-mediated plasticity of the synaptic device. (f)–(i)[242] John Wiley & Sons. © 2023 Wiley-VCH GmbH. [Illustrations in (a) Created in BioRender. Son, D. (2025) https://BioRender.com/f95i862.].

spin-coated PEDOT:PSS film served as a channel layer, and a chemically responsive ionogel gate electrolyte completed a flexible synaptic device (Figure 7(b))[241]. The device mimics the physical structure of a biological olfactory synapse: the gate electrode, ionogel, channel, and source/drain electrodes correspond to the presynaptic membrane in an inhibitory interneuron of a periglomerular cell (PGC), the presynaptic membrane in an olfactory receptor neuron (ORN), the chemical synapse, and the postsynaptic membrane in a projection neuron (PN). In this system, cations and anions act as the inhibitory neurotransmitter gamma-aminobutyric acid (GABA) and the excitatory neurotransmitter glutamate, respectively, in the synaptic device. The device generates excitatory or inhibitory postsynaptic signals in biological olfactory synapses, and the corresponding complex details activated by neurotransmitters are transmitted to postsynaptic receptors, which modulate the functions of learning and forgetting. By emulating the mechanism of the olfactory perception system, the artificial chemoreceptive device demonstrates capabilities such as sensing, learning, forgetting, and modulating signals as electrochemical olfactory synapses. The postsynaptic output current was reliably controlled by exposure to NO_2 gas, which enhanced excitatory action potentials in proportion to the concentration of the target molecule, and by gate voltage, which elicited inhibitory action potentials (Figure 7(c)). In addition to distinguishing the concentration of the target molecule, the post-synaptic output current of the artificial olfactory synapse reliably increased as a function of the exposure frequency to NO_2 gas (Figure 7(d)). The device also demonstrated increased postsynaptic output

current with repeated NO_2 exposure, reinforcing synaptic plasticity through increased synaptic weight (Figure 7(e)).

In another example, a soft organic electrochemical synaptic device was fabricated using deposited Au electrodes, spin-coated PEDOT:PSS channels, and a porous solid polymer electrolyte (SPE) film produced using the breath figure method (Figure 7(f))[242]. The breath figure method utilizes condensed water droplets in a humid environment as sacrificial templates to produce a microporous structure that enhances the effective area of gas interaction, thereby improving device sensitivity. The device was fabricated on a polyethylene terephthalate (PET) substrate to implement a flexible artificial olfactory synapse. In biological synapses, the transition from short- to long-term potentiation is driven by neurotransmitter molecules released by exocytosis from presynaptic cells and bound to postsynaptic receptors. This chemical synaptic device is inspired by a gasotransmitter-mediated plasticity mechanism. The operational mechanism for the transition from short- to long-term potentiation in the device employs excessive H_2S molecules, which are known to be toxic materials causing adverse health effects, trapped in the SPE layer, where cations from the electrolyte are irreversibly transported into the PEDOT:PSS channel. The large effective area for chemical interaction of the device enables the detection of target molecules with sensitivity down to parts per billion (ppb) and selectivity over other gases. The sensing performance of the device was experimentally verified by distinguishing concentration differences of H_2S gas at 5 ppm (parts per million) (Figure 7(g)). The main purpose of this biomimetic facial synapse is to augment the function of the natural human olfactory perception system, which does not respond well to long-term or excessive exposure due to fatigue of biological perception, often caused by the detriment of epithelial receptors. Therefore, the required functionalities for assistive artificial perception include both sensing capabilities and recognition of specific chemicals. The device demonstrated short-term memory (STM) to long-term memory (LTM) transition driven by H_2S stimuli, leading to increased synaptic weight (Figure 7(h)). It was verified that the synaptic weight was reliably reinforced by an increased concentration of the target molecule, while the exposure time was constant. With these high sensing capabilities and reliable synaptic properties, the device demonstrated a proportional real-time output response (Figure 7(i), upper graph) and corresponding synaptic weight changes (Figure 7(i), lower graph) as a function of the input voltage, which verified the gasotransmitter-mediated plasticity.

5. Neuromorphic sensorimotor loop system for closed-loop neuroprosthetics

In biological systems, sensory perception and motor execution are linked through numerous synaptic clefts that complete the sensorimotor loop pathway. This neural circular system detects external stimuli via sensory receptors, processes signals in the brain, and transmits motor commands to muscles, which generate feedback based on newly updated sensory stimuli induced during continuous exercise (Figure 8(a)). Sensory feedback signals during physical actions play an important role in providing feedback that helps the brain make continuous adjustments, ensuring that the body meets its original goals and avoids issues such as insufficient muscular fatigue. Multiple synaptic connections in the sensorimotor loop also contribute to energy efficiency, speed, and accuracy by enabling low-power signal processing, transmission, and memory storage, which support learning and adaptive responses based on past experiences. Considering these properties, neuroprosthetics as substitutes for biological sensorimotor functions aim to integrate closed-loop systems with sensory feedback and neuromorphic computing that incorporates biomimetic artificial synapses to replicate sensorimotor functions.

In terms of recent technological advancements in practical and clinical applications, closed-loop prosthetic limbs have been developed to emulate the natural integration of sensory units and fine actuators bridged by intercurrent perception feedback[246–264]. A notable example is a closed-loop robotic-arm system that features prosthetic control using neural feedback based on real-time force and slippage sensations[243]. This system incorporates EMG electrodes, a force-sensing resistor, and a combination of cuff and intraneural electrodes. These components are organically connected, and their functionalities are mobilized to build a closed-loop operation (Figure 8(b)). In the operational sequence, the motor intentions of patients are detected as muscle activities by EMG sensors and decoded through a pattern recognition algorithm that classifies the gesture and force scale. This controls the position and force of the artificial limb during task execution. During actuation of the robotic arm, the force sensor integrated into the fingers detects force and slippage events that occur when contacting objects, resulting in the provision of feedback information by encoding nerve stimulation patterns that correspond to the applied sensations. The electrical sensory signal initiated by the force sensor device is transmitted to the patient's natural biological system through peripheral nerve-interfaced electrodes, causing the patient to perceive the applied force and slipperiness of the interacting substances. The delivery process of the sensory stimuli is important in that the sensory feedback ultimately leads to closed-loop motor control, allowing the patients to adjust the fine motion of the artificial limb based on recognized information relating to how much force is applied to the objects in contact and how reliably the user interacts with them as intended. It was demonstrated that a patient equipped with a prosthesis capable of neural feedback performed better at manipulating tasks involving small objects using the fingers of an artificial hand than a patient without feedback functionality (Figure 8(c)). By utilizing the information regarding the applied force and slippery level induced by interaction with a substance as the sensation feedback, the patient with the closed-loop robotic limb was able to engage in a more natural posture, prompt motion occurrence, and delicate force adjustment. In contrast, a patient lacking sensation feedback struggles with stable gripping and accurate control. It

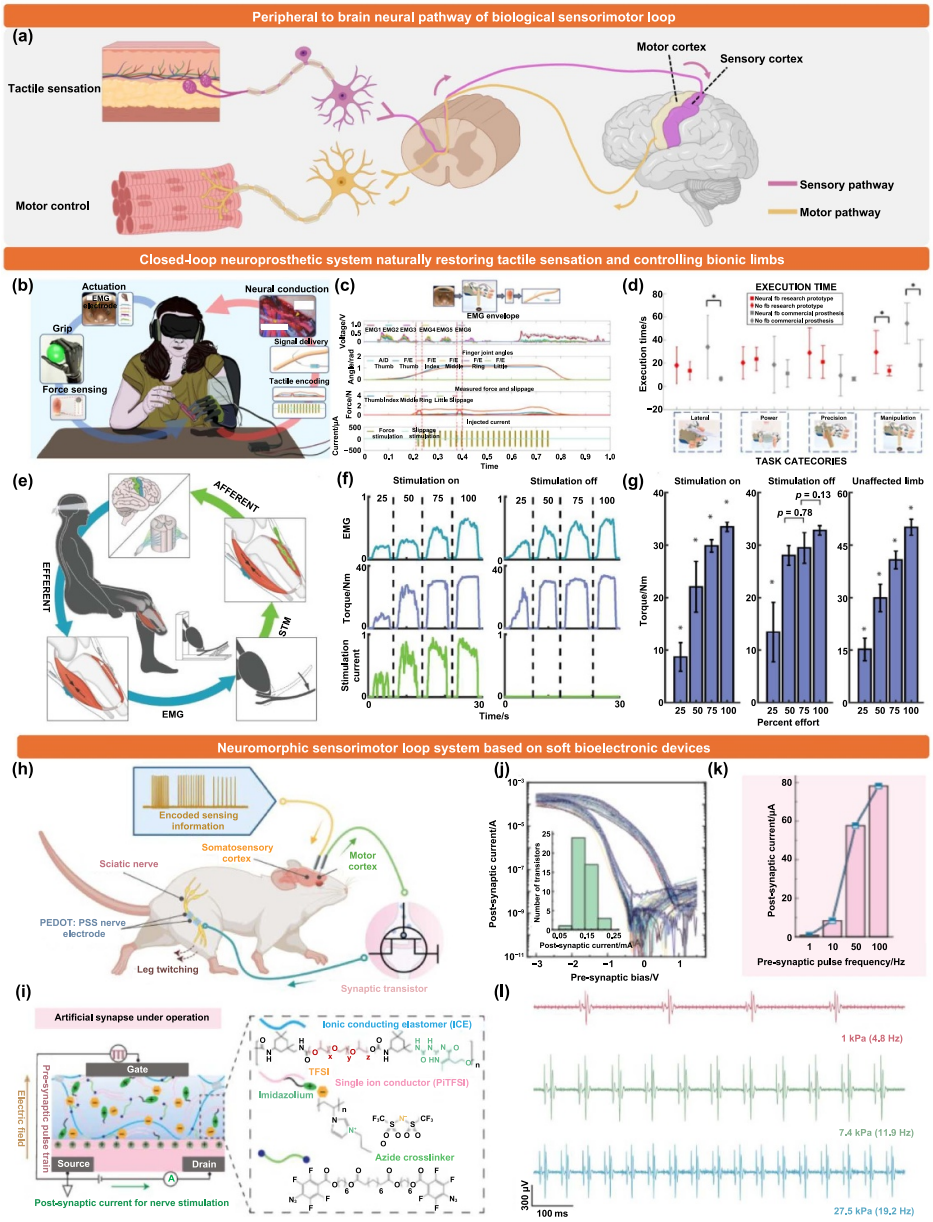

Figure 8. Soft neuromorphic sensorimotor loop system incorporating an artificial synapse for closed-loop neuroprosthetic technology. (a) Schematic of the biological sensorimotor loop system. Tactile sensory transmission from mechanoreceptors to the brain and perception at the sensory cortex induce motor feedback elicited from the motor cortex to muscles via synapses. (b)–(g) Closed-loop neuroprosthetic systems for natural restoration of tactile sensation and spontaneous control of bionic limb actuation utilizing sensory feedback. (b) Schematic of the operational flow of real-time closed-loop control of the prosthetic upper limbs using force-and-slippage sensory feedback obtained by neural interfacing electrodes. (c) Real-time measurement of the EMG amplitude, finger angle, and force level by producing different EMG signals during closed-loop force and slippage control of the manipulation task of a shape sorter of a small cylindrical object. (d) Measured weighted success for various categories, including lateral, power, precision, and manipulation, regarding task performance while grasping objects using closed-loop prosthetic control. (b)–(d) From[243]. Reprinted with permission from AAAS. (e) Schematic of closed-loop torque control of the prosthetic lower limb utilizing restored proprioception feedback facilitated by AMI. (f) Representative measurement of lateral gastrocnemius EMG (blue) and torque (purple) signals during different stimulation currents (green) in closed-loop torque control for the "stimulation on" (n = 79 total trials) and "stimulation off" (n = 79 total trials) trial cases respectively. The numbers at the top of the graph correspond to the percentages of the effort commands. (g) Mean data of measured torque signals for the trials of closed-loop prosthetic control in each of the "stimulation on," "stimulation off," and "unaffected limb" (n = 80 trials) cases. (e)–(g) From[244]. Reprinted with permission from AAAS.(h)–(l) Neuromorphic sensorimotor loop system integrated with soft bioelectronic devices. (h) Schematic illustrating the artificial sensorimotor loop system applied to living animals. (i) Schematic of the structure and working mechanism of a soft stretchable synaptic transistor. The active domain of a fully solid-state artificial synapse utilizes an organic semiconductor channel and a solid-state ionic dielectric composed of ICE with high ion conductivity, azide crosslinkers, and a single-ion conductive PiTFSI. (j) Transfer curves of synaptic transistors and the distribution of post-synaptic current (inset) for the synaptic transistor array. (k) Correlation plot showing the relationship between presynaptic pulse train frequency and the corresponding amplitude of the post-synaptic current obtained from a synaptic transistor. (l) Feedback signals recorded from the motor cortex elicited by different pressures applied to a tactile sensor embedded in soft e-skin. (h)–(l) From[245]. Reprinted with permission from AAAS. [Illustrations in (a) Created in BioRender. Son, D. (2025) https://BioRender.com/d76k984.].

was also verified that the utilization of tactile feedback information elicited during motor activities improves exercise accuracy and execution efficiency comprehensively for performing actions, including the exertion of force on objects and interaction with them in various ways, not limited to the case of one manner of object manipulation (Figure 8(d)).

Another representative technology involves lower-limb applications. The system features an agonist-antagonist myoneural interface (AMI) methodology for restoring proprioception, which is the ability to sense the relative spatial positioning of body parts and the amount of force exerted on objects or the environment[244]. Proprioception is critical for delicate motor control, gait adaptation, and joint stability and this study emphasizes its use as sensory feedback information in bionic joints. This function is embedded in the prosthetic system, where agonist and antagonist muscle tendons are connected mechanically in series and exhibit AMI (Figure 8(e)). The ultimate scheme of the closed-loop robotic lower limb applied to an amputee is aimed at natural torque control. Afferent feedback of the prosthetic joint torque is delivered through functional electrical stimulation (FES) to the antagonist muscle, enabling the subject to perceive artificial stimulation from the EMG sensors as a natural sensation of ankle torque. It was demonstrated that the torque control of the robotic limbs with closed-loop feedback replicating proprioceptive sensation, enabled the segmentation and linearization of torque force as a function of the effort ratio proportional to the EMG level, a feature more distinct than that of systems lacking proprioceptive feedback (Figures 8(f) and (g)).

The latest state-of-the-art neuroprosthetic technologies have improved functionality through the use of closed-loop systems; however, their clinical application remains limited. The absence of synaptic devices that mimic biological neurons using neuromorphic computation contributes to the incompatibility of prosthetic-neural interfaces[265−282]. Consequently, artificial perception systems with biomimetic synapses have yet to be fully implemented due to technical challenges. One crucial challenge is the need for electronic systems, designed to replicate a series of biological functions, to be seamlessly integrated with soft materials and devices[283−285]. The discrepancy between the technical difficulty of demonstrating hardware-implemented neuromorphic computations and the relatively mature field of soft electronics further hinders progress toward this goal. A subsequent study reported a neuromorphic system that incorporated artificial synaptic devices made from soft electronic materials[245]. To date, this remains the only system-level demonstration of soft electronics with closed-loop neuromorphic functions, designed to mimic the biological circulation system. This bioelectronic system developed in a soft and fully stretchable form incorporates skin sensors, a processing circuit combining a ring oscillator and an edge detector, and a synaptic transistor connected with a nerve-interfacing electrode that embodies the biological sensorimotor loop. The soft neuromorphic framework was applied to a living animal, demonstrating closed-loop sensory perception and motor control (Figure 8(h)). Within a set of functions, the perceptual process is initiated by the sensation of external tactile stimuli applied to artificial receptor devices, including pressure and temperature sensors. The detected analog tactile signals are sequentially digitized and encoded through a series of ring oscillators and edge detector circuits, converting and reshaping them into spike-like signal trains, where different amplitudes of the input pressure stimuli are encoded into different frequencies of the output pulse train. This operation emulates the function of biological sensory receptors, where signal transduction occurs from physical information to an authentic bioelectricity modality. Encoded spikes containing frequency information are delivered to the sensory cortex using a probe electrode, resulting in sensory perception and motor plan promotion. Neural activities corresponding to motor commands generated from the motor cortex flow into the soft artificial synaptic transistor to be processed and converted into a postsynaptic current, whose signal pattern emulates that of natural motor activity. The soft, intrinsically stretchable, fully solid-state synaptic transistor newly developed in the study employs an active layer incorporating an organic semiconductor channel that leverages the nanoconfinement effect and a solid-state ionic dielectric made from ionic conducting elastomer (ICE) with high ion conductivity, azide crosslinkers, and a single-ion conductive polyelectrolyte {poly[(1-vinyl-3-propyl-imidazolium) bis(trifluoromethanesulfonyl)imide] (PiTFSI)} (Figure 8(i)). The artificial synapse exhibited a large hysteresis in the transfer curves maintained under 50% strain (Figure 8(j)). Furthermore, the synaptic transistor caused large changes in the amplitudes of the postsynaptic currents as a function of the gate input frequency. An approximately 4-order-of magnitude output difference occurred with presynaptic pulses of different frequencies between 1 and 100 Hz (Figure 8(k)), whereas the all-solid-state devices maintained a stable postsynaptic current with no significant variation after soaking in physiological fluids for hours. Using mechanoreceptor-inspired sensory encoding circuits and synaptic transistors, a neuromorphic sensorimotor loop system was developed and applied to an anesthetized small-animal model *in vivo*. Spike pulse trains, as sensory signals encoded by the biomimetic circuits embedded in the soft stretchable electronic skin system, were transmitted by a series of output nodes of the circuits, an amplifying buffer, and a platinum (Pt) wire electrode, stimulating the somatosensory cortex of the animal, which elicited responsive spikes from the motor cortex recorded by another wire electrode. It was experimentally demonstrated that stronger pressure applied to the prosthetic e-skin reliably led to faster motor feedback (Figure 8(l)). Presynaptic spikes with different frequencies, output from the motor cortex, and subsequently input into the gate node of the synaptic transistor resulting in a postsynaptic output current with proportional amplitude. This

current stimulated the sciatic nerve and modulated the degree of muscle activity by different amplitudes of motor feedback using an interfaced PEDOT:PSS nerve electrode. These results are significant as they represent the feasibility of hardware implementation of closed-loop neuromorphic prostheses, as well as their real-time operation in live animals.

6. Perspective

In this review, we comprehensively investigated the recent technological progress in perception-mimicking systems integrated with artificial receptors and synapses for the implementation of advanced neuroprosthetics. We organized the literature according to the following scope and objectives: as described above, a closed-loop neuroprosthetic technology capable of functionally replacing significantly damaged or completely lost natural limbs and sensory organs is essential for the development of customized prosthetics. It is also important to develop bidirectional systems incorporating electromechanical exoskeletons and control circuitry to provide motor functions as well as sensors, transducers, and transmission circuitry to reproduce perceptions. These bilateral functionalities must be connected and circulated, while including sensory feedback, similar to the mechanisms of the human body. However, achieving successful hardware implementation of a comprehensive prosthetic system for customized and biologically compatible applications remains a significant challenge. Thus, the development of prosthetic systems involves various strategies for implementing hardware units, each aimed at performing specific roles.

Sensors based on soft materials, designed to be embedded within the artificial skin of prosthetic appliances for the input of external stimuli, were primarily introduced as imitational sensory receptors. Recent advances in prosthetic systems have led to the development of sensor devices with soft form factors. The objective of such platforms is to reproduce sensations and create artificial skin with mechanical properties that are both aesthetically and functionally compatible with the original skin. Although significant advances have been made in developing highly functional soft-sensor devices compatible with CMOS technology and peripheral IC systems, artificial receptors have mainly been studied based on independent sensor devices designed to detect external stimuli using flexible and stretchable materials. The latest applications of these artificial sensory systems in prosthesis technology have been combined with AI software supported by high-performance computing systems. These systems perform online neural network-based learning and inference to process electrophysiological signals and enhance sensing performance.

Furthermore, to fully substitute biological systems and restore physiological functions using artificial bidirectional systems, it is essential to implement a closed-loop operation comprising hardware-implemented high-performance processors. These devices require capabilities for data computation and storage, similar to biological nervous systems, while providing low-power parallel processing and synaptic plasticity. In this context, the latest neuromorphic compute-in-memory systems emulate the operational mechanisms of the human brain by integrating conventional CMOS memory, including SRAM, and futuristic memristors employing emerging non-volatile memory technologies such as RRAM. However, because these systems were not developed specifically to process electrophysiological signals in biological systems, they are not optimized to replicate the structure and operational mechanisms of neural pathways related to sensory perception and motor control in terms of system configuration and circuitry design. Consequently, biomimetic sensory-prosthetic systems employing soft neuromorphic devices based on artificial synapses have emerged as promising solutions. These synaptic devices, which can be classified into two- or three-terminal nodes, employ various operating methods depending on their physical structure and material strategies. They exhibit different strengths in metrics such as operation voltage, switching speed, voltage window, endurance, and retention time, which determine the performance of large-scale artificial synapse arrays and fully hardware-implemented neuromorphic systems. These systems are evaluated based on integration density, complexity of the circuitry, conductance level, energy per operation, and other factors. These synaptic devices can be manufactured as flexible or stretchable platforms with mechanical softness by incorporating appropriate material strategies and fabrication protocols, making them highly compatible with receptor-mimicking soft sensors while maintaining both computation and storage capabilities with low power consumption.

Building on these developments, soft sensory-neuromorphic systems have been developed to emulate perception and memorization processes. These systems detect external stimuli with artificial receptors, process analog input signals into spikes, and perform synaptic plasticity. The literature on recent sensory-neuromorphic systems incorporating soft artificial synapses, as introduced in this review, verifies the feasibility of various artificial perceptions, including those for vision, olfaction, and tactile sensing. In particular, it has been demonstrated that sensors and synaptic devices with soft, flexible, and stretchable properties enable perception prostheses to interface conformally with biological tissues. This indicates that artificial perception systems can be compatibly embedded within the prosthetic skin of robotic limbs or combined with extremely soft tissues, such as the retina, while reproducing the same mechanical behavior as the original body without functional and aesthetic incompatibility. Despite these significant advancements, research in the field of soft and deformable electronics has primarily focused on discovering optimal materials and ensuring both mechanical and electrical stabilities at the individual device level. Given the current state of technology, there are relatively few examples of array-scale artificial synaptic devices implemented in flexible or stretchable form factors. Consequently, the challenges in advancing soft neuromorphic hardware based on artificial synapses for perception-reproducible neuroprosthetics are as follows:

First, in addition to improving performance, it is essential for synaptic devices to ensure durability, repeatability, and lifetime under continuous electrical operation and mechanical deformation. These qualities are key merits for the long-term usability of prosthetics. To meet these requirements, the soft electronic materials mobilized to develop artificial synapses—including inorganic thin films, nanoparticles and nanowires, elastomers, and solid-state electrolytes—must be advanced to maintain stable performance over extended periods. Additionally, these materials must be compatible with large-area, high-throughput, uniform, and high-quality manufacturing methods. By applying mechanically stable materials and compatible manufacturing processes, soft synaptic devices can become scalable, durable, and reliable, making them suitable for extended use in prosthetics.

Second, in addition to the device technology for artificial synapses mimicking visual, tactile, and olfactory perception which are mainly introduced in the manuscript, efforts to implement other synaptic devices included in the five senses with soft and flexible form factors are also very essential for complete neuromorphic prosthetic system. Regarding hearing and taste, the advancement of synaptic device technology for replicating those senses in terms of deformable platforms is at an early stage, where most of the developed devices have been fabricated to rigid form factors[286−290]. To date, auditory and gustatory sensation-recognizing synaptic devices with mechanical deformation properties integrated based on flexible electronic materials have emerged in the latest reports[291,292]. In the case of artificial synapses for the auditory system, both sensor devices as the receptor transducing mechanical vibration into an electrical aural signal and synaptic devices for processing the converted electrical signals should be fabricated as a mechanically deformable form factor and physically integrated with each other. On the other hand, gustatory-mimicking devices operate by detecting chemical molecules and converting them into electrical signals for synaptic processing, which is similar to that of artificial olfactory synapses. However, there is a fundamental difference that the olfactory system detects gaseous chemicals while the gustatory system captures liquid chemicals, which makes it difficult to implement artificial synapses emulating taste perception due to the requirement of material and device stability under liquid conditions. In order to overcome these barriers to advance auditory and gustatory synaptic devices, breakthroughs in related technical elements including novel soft electronic materials, design of reliable and stable device structure, and integration process of deformable platforms would be comprehensively required.

In addition to the overall development of artificial synaptic devices for each five-sensory perception, implementation of the multimodal perception-replicating system, which is capable of integrating multiple sensory inputs and processing them to perceive complex sensation without any distortion and interference in information, would be the ultimate goal of the complete network of artificial synapses. In the living system, the thalamus and the association cortex of the brain are respectively responsible for integrating and processing detailed sense information in the same type delivered from each specific receptor (e.g. tactile inputs including pressure, temperature, texture, and pain) resulting in sophisticated unisensory perception and different type of sense information transmitted from each primary cortex (e.g. five-sense inputs including vision, touch, hearing, smell, and taste) leading to multi-sensory perception. Inspired by these biological operations, there have been primary development of soft multimodal synaptic devices which can process different input information by connecting with multiple sensor devices of different modalities[293−301]. Despite significant advances, it is very difficult to develop a genuine multimodal synaptic device capable of merging different sensory information, decoupling them, and performing variable synaptic operations based on the appropriate weight of each information. In addition, the progress so far has not reached the natural imitation of complex and hierarchical neurotransmission and processing pathways, but rather has achieved primitive implementations inspired by the operational mechanism of biological nervous system. It would also be significant challenges to functionalize these multimodal synaptic devices to be soft and deformable and to ensure compatibility with scalable process technology. To realize the ultimate goal, therefore, the development of both *in-situ* multi-sensory processible soft synaptic devices and system-level configuration should be accompanied.

After successfully replicating or restoring the biological sensory systems of humans, the next essential step in prosthetic technologies is to explore the augmentation of human abilities beyond these senses. By leveraging artificial neuromorphic systems to explore additional sensory modalities inspired by unique biological mechanisms in nature (e.g. insects, animals, etc.), such as magnetoreception, electroreception, and ultrasound detection, higher reaction speeds and sensitivities can be achieved[302−305]. This approach holds significant potential for advancing future supreme human-machine interface technologies.

In this respect, comprehensive and tailored strategies for advancing neuromorphic systems based on artificial synapses have yet to be fully developed. After improving individual synaptic devices with optimal device structures and material engineering, efforts must focus on replicating the biological configuration of trillions of neurons and synapses within neural pathways. This includes the summation, conversion, transmission, and storage of sensory or motor signals with low power. To scale up bioinspired beyond-CMOS devices to the array level and integrate them with existing CMOS-based peripheral systems, compatible circuitry based on artificial synapse arrays, multistep fabrication protocols designed for compatible circuit layouts, and optimization of unit processes using unconventional materials and process integration are required. These challenges necessitate extensive contributions from experts in physical, chemical, biological, and electrical engineering.

Finally, with scalable hardware-implemented synaptic devices and circuits, the construction of a neural computation model and the embedding of operational firmware within the complete hardware is the final challenge in completing

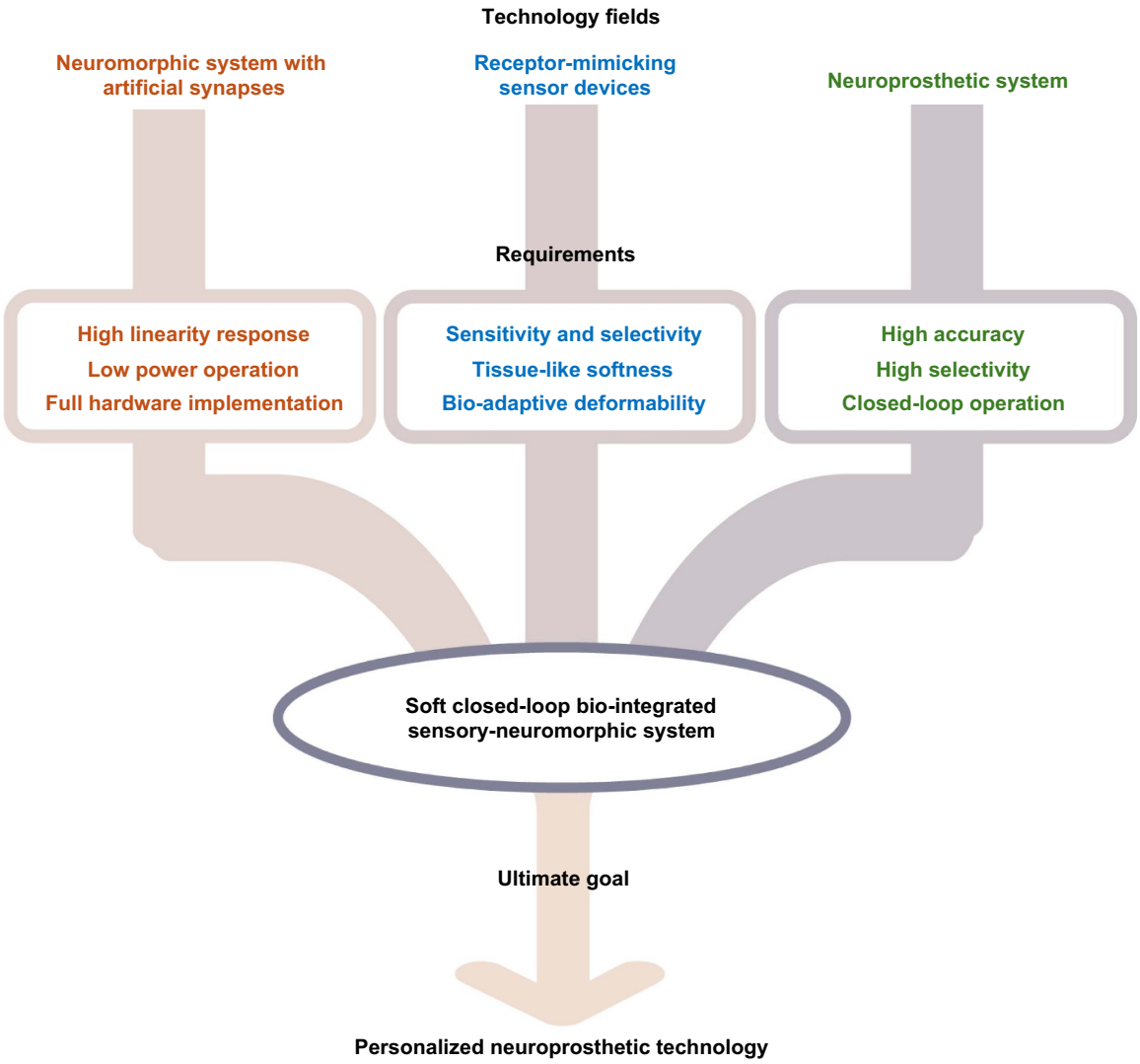

Figure 9. Key element technologies for realizing the ultimate bio-integrated closed-loop soft neuromorphic human prosthesis. Various technical requirements from each field are essential for achieving technology fusion. The ultimate goal is the development of tailor-made systems personalized for individuals, considering their unique physical characteristics, as well as motor and cognitive abilities.

an authentic neuromorphic prosthetic system. While significant advances have been made, a deeper understanding of biological neural pathways and innovative developmental skills based on computer science and engineering are needed to complete the optimal model. Specifically, for closed-loop operations with continuous feedback signals similar to those of the human body, additional connections and designs of the aforementioned sensors and synaptic circuits to separate feedback systems are required to ensure precise perception of external stimuli and corresponding motor actuations. Furthermore, it is worth noting the importance of a long-term stable power supply for systems where sensors and processors are well-integrated. While conventional prosthetics and robotics have relied on rigid, bulky batteries for operation, recent advancements in wearable power supplies have focused on developing soft, skin-like form factors using technologies such as triboelectric nanogenerators (TENG) and thermoelectric generators (TEG)[306 – 309]. However, these skin-like batteries face limitations in implementing closed-loop feedback systems for prosthetics due to their short lifespan and low efficiency. In contrast, battery-less systems, which deliver power externally via antennas or coils, offer the advantage of providing power on demand, making them promising candidates for wearable and implantable applications[310,311]. Recent studies have specifically focused on creating stretchable tags and readers that can efficiently and accurately deliver power and information wirelessly, even during continuous motion or daily activities[312]. If a proper combination of soft batteries, wireless power transmission, and stretchable charge-delivering circuits is achieved, it would enable the neuromorphic systems implemented earlier to operate more stably and over a longer duration. This advancement would contribute to making prosthetics more convenient and capable of mimicking human-like movements more closely. Ultimately, portable automated neuromorphic systems can be created once both hardware and software are designed and optimized.

The schematic shown in Figure 9 illustrates the blueprints for closed-loop neuromorphic prosthetic technology. The final

objective of this technological fusion is to directly connect with human nerves and perfectly reproduce the appearance and function of the original sensory organs and limbs. Each technology involved must not only advance but also operate cohesively as part of a unified system. To implement bidirectional artificial neural pathways in hardware, the development of soft sensory-neuromorphic systems and the corresponding soft motor neuromorphic systems should be advanced. A complete closed-loop neuromorphic prosthesis is achieved when these bilateral neuromorphic functionalities are embedded into the system, connected through hardware and software, and controlled in series and parallel. Furthermore, achieving direct integration of the artificial body with the nerve requires a neural interface technology that avoids damaging or causing inflammatory side effects to nerve tissues, which are characterized by low modulus and stiffness, and flexible, stretchable behaviors. Functionally, high-speed link technology is crucial to enable communication between nerves and electronics, multiplexed electrical signals with wide bandwidth, and high-throughput capabilities while minimizing artifacts and interference. Despite the numerous challenges, the development of closed-loop soft neuromorphic prosthetic systems is highly promising and is expected to have a profound impact. We hope this review provides insights and perspectives for researchers in this field.

Acknowledgment

This research was supported by the National Research Foundation of Korea (NRF) grant funded by the Korean government (MSIT) (No. 2020R1C1C1005567). This study was also supported by the NAVER Digital Bio Innovation Research Fund, funded by NAVER Corporation (Grant No. [37-2023-0040]). This work was supported by Institute of Information & communications Technology Planning & Evaluation (IITP) grant funded by the Korea government (MSIT) (No. 2020-0-00261, Development of low power/low delay/self-power suppliable RF simultaneous information and power transfer system and stretchable electronic epineurium for wireless nerve bypass implementation). This research was also supported by Institute for Basic Science (IBS-R015-D1, IBS-R015-D2). This research was supported by a grant of the Korea-US Collaborative Research Fund (KUCRF), funded by the Ministry of Science and ICT and Ministry of Health & Welfare, Republic of Korea (Grant Number. RS-2024-00467213). Figures 1, 2(a), 5(a), 6(a), 7(a), and 8(a) were created using Biorender.com.

Author contributions

J K, S L, and J Y contributed equally to this work. J K, S L, J Y, and D S wrote the manuscript and participated in the modification.

The authors declare that there is no conflict of interest regarding the publication of this paper.

ORCID iD

Donghee Son https://orcid.org/0000-0002-3772-8009

References

[1] Finch J. 2011. The ancient origins of prosthetic medicine. *Lancet* **377**, 548–549.
[2] Lai J H and Hodges J S. 1999. Effects of processing parameters on physical properties of the silicone maxillofacial prosthetic materials. *Dent. Mater.* **15**, 450–455.
[3] Cimolato A, Driessen J J M, Mattos L S, De Momi E, Laffranchi M and De Michieli L. 2022. EMG-driven control in lower limb prostheses: a topic-based systematic review. *J. Neuroeng. Rehabil.* **19**, 43.
[4] Rodríguez-Tapia B, Soto I, Martínez D M and Arballo N C. 2020. Myoelectric interfaces and related applications: current state of EMG signal processing–a systematic review. *IEEE Access* **8**, 7792–7805.
[5] Ahkami B, Ahmed K, Thesleff A, Hargrove L and Ortiz-Catalan M. 2023. Electromyography-based control of lower limb prostheses: a systematic review. *IEEE Trans. Med. Robot. Bionics* **5**, 547–562.
[6] Lee S et al. 2020. Wireless epidermal electromyogram sensing system. *Electronics* **9**, 269.
[7] Xiong D Z, Zhang D H, Zhao X G and Zhao Y W. 2021. Deep learning for EMG-based human-machine interaction: a review. *IEEE/CAA J. Autom. Sin.* **8**, 512–533.
[8] Ko H, Kim S, Lee E and Kim E. 2024. Leveraging artificial intelligence in the bioengineering of prosthetics: enhancing athletic performance and accessibility for disabled athletes through adaptive, smart prosthetic technologies. *J. Artif. Intell. Res.* **4**, 1–30. https://thesciencebrigade.com/JAIR/article/view/308.
[9] Mastinu E, Doguet P, Botquin Y, Håkansson B and Ortiz-Catalan M. 2017. Embedded system for prosthetic control using implanted neuromuscular interfaces accessed via an osseointegrated implant. *IEEE Trans. Biomed. Circuits Syst.* **11**, 867–877.
[10] Son D et al. 2018. An integrated self-healable electronic skin system fabricated via dynamic reconstruction of a nanostructured conducting network. *Nat. Nanotechnol.* **13**, 1057–1065.
[11] Song J K et al. 2017. Wearable force touch sensor array using a flexible and transparent electrode. *Adv. Funct. Mater.* **27**, 1605286.
[12] Kim S, Jang J, Kang K, Jin S B, Choi H, Son D and Shin M. 2023. Injection-on-skin granular adhesive for interactive human–machine interface. *Adv. Mater.* **35**, 2307070.
[13] Thomas T and Kurian A N. 2022. Robotic technology in the development of prosthesis. *In Machine Learning for Critical Internet of Medical Things: Applications and Use Cases* eds Al-Turjman F and Nayyar A (Springer, Cham) pp 153–175.
[14] Babu D, Nasir A, Ravindran, Farag M and Jabbar W A. 2023. 3D printed prosthetic robot arm with grasping detection system for children. *Int. J. Adv. Sci. Eng. Inf. Technol.* **13**, 226–234.

[15] Bajaj N M, Spiers A J and Dollar A M. 2019. State of the art in artificial wrists: a review of prosthetic and robotic wrist design. *IEEE Trans. Robot.* **35**, 261–277.
[16] Lee W W, Tan Y J, Yao H C, Li S, See H H, Hon M, Ng K A, Xiong B, Ho J S and Tee B C K. 2019. A neuro-inspired artificial peripheral nervous system for scalable electronic skins. *Sci. Robot.* **4**, eaax2198.
[17] Du J, Vann W, Zhou T Y, Ye Y and Zhu Q. 2024. Sensory manipulation as a countermeasure to robot teleoperation delays: system and evidence. *Sci. Rep.* **14**, 4333.
[18] Kim D H et al. 2011. Epidermal electronics. *Science* **333**, 838–843.
[19] Kim Y G, Song J H, Hong S and Ahn S H. 2022. Piezoelectric strain sensor with high sensitivity and high stretchability based on kirigami design cutting. *npj Flex. Electron.* **6**, 52.
[20] Yang Y R et al. 2020. A laser-engraved wearable sensor for sensitive detection of uric acid and tyrosine in sweat. *Nat. Biotechnol.* **38**, 217–224.
[21] Wen F, Zhang Z X, He T Y Y and Lee C. 2021. AI enabled sign language recognition and VR space bidirectional communication using triboelectric smart glove. *Nat. Commun.* **12**, 5378.
[22] Zhou Z H et al. 2020. Sign-to-speech translation using machine-learning-assisted stretchable sensor arrays. *Nat. Electron.* **3**, 571–578.
[23] Loke G et al. 2021. Digital electronics in fibres enable fabric-based machine-learning inference. *Nat. Commun.* **12**, 3317.
[24] Sipola T, Alatalo J, Kokkonen T and Rantonen M. 2022. Artificial intelligence in the IoT era: a review of edge AI hardware and software. *In 2022 31st Conference of Open Innovations Association (FRUCT)*. (IEEE, Helsinki, Finland) pp 320–331.
[25] Wei Y, Zhou J, Wang Y, Liu Y G, Liu Q S, Luo J S, Wang C, Ren F B and Huang L. 2020. A review of algorithm & hardware design for AI-based biomedical applications. *IEEE Trans. Biomed. Circuits Syst.* **14**, 145–163.
[26] Manickam P, Mariappan S A, Murugesan S M, Hansda S, Kaushik A, Shinde R and Thipperudraswamy S P. 2022. Artificial intelligence (AI) and internet of medical things (IoMT) assisted biomedical systems for intelligent healthcare. *Biosensors* **12**, 562.
[27] Du Nguyen H A, Yu J T, Xie L, Taouil M, Hamdioui S and Fey D. 2017. Memristive devices for computing: beyond CMOS and beyond von Neumann. *In 2017 IFIP/IEEE International Conference on Very Large Scale Integration (VLSI-SoC)*. (IEEE, Abu Dhabi, United Arab Emirates) pp 1–10.
[28] Sebastian A, Le Gallo M, Khaddam-Aljameh R and Eleftheriou E. 2020. Memory devices and applications for in-memory computing. *Nat. Nanotechnol.* **15**, 529–544.
[29] Chen W-H et al. 2019. CMOS-integrated memristive non-volatile computing-in-memory for AI edge processors. *Nat. Electron.* **2**, 420–428.
[30] Xue C X et al. 2021. A CMOS-integrated compute-in-memory macro based on resistive random-access memory for AI edge devices. *Nat. Electron.* **4**, 81–90.
[31] Roy K, Jaiswal A and Panda P. 2019. Towards spike-based machine intelligence with neuromorphic computing. *Nature* **575**, 607–617.
[32] Shastri B J, Tait A N, Ferreira de Lima T, Pernice W H P, Bhaskaran H, Wright C D and Prucnal P R. 2021. Photonics for artificial intelligence and neuromorphic computing. *Nat. Photon.* **15**, 102–114.
[33] Marković D, Mizrahi A, Querlioz D and Grollier J. 2020. Physics for neuromorphic computing. *Nat. Rev. Phys.* **2**, 499–510.
[34] Rao A, Plank P, Wild A and Maass W. 2022. A long short-term memory for AI applications in spike-based neuromorphic hardware. *Nat. Mach. Intell.* **4**, 467–479.
[35] Donati E and Indiveri G. 2023. Neuromorphic bioelectronic medicine for nervous system interfaces: from neural computational primitives to medical applications. *Prog. Biomed. Eng.* **5**, 013002.
[36] Rajendran B, Sebastian A, Schmuker M, Srinivasa N and Eleftheriou E. 2019. Low-power neuromorphic hardware for signal processing applications: a review of architectural and system-level design approaches. *IEEE Signal Process. Mag.* **36**, 97–110.
[37] Kim J, Im J, Shin W, Lee S, Oh S, Kwon D, Jung G, Choi W Y and Lee J H. 2024. Demonstration of in-memory biosignal analysis: novel high-density and low-power 3d flash memory array for arrhythmia detection. *Adv. Sci.* **11**, 2308460.
[38] Zeng M Y, He Y L, Zhang C X and Wan Q. 2021. Neuromorphic devices for bionic sensing and perception. *Front. Neurosci.* **15**, 690950.
[39] Kennedy M B. 2016. Synaptic signaling in learning and memory. *Cold Spring Harb. Perspect. Biol.* **8**, a016824.
[40] Kotaleski J H and Blackwell K T. 2010. Modelling the molecular mechanisms of synaptic plasticity using systems biology approaches. *Nat. Rev. Neurosci.* **11**, 239–251.
[41] Deckers L, Van Damme L, Van Leekwijck W, Tsang I J and Latré S. 2024. Co-learning synaptic delays, weights and adaptation in spiking neural networks. *Front. Neurosci.* **18**, 1360300.
[42] Magee J C and Grienberger C. 2020. Synaptic plasticity forms and functions. *Annu. Rev. Neurosci.* **43**, 95–117.
[43] Morrison A, Diesmann M and Gerstner W. 2008. Phenomenological models of synaptic plasticity based on spike timing. *Biol. Cybern.* **98**, 459–478.
[44] Wan Q Z, Sharbati M T, Erickson J R, Du Y H and Xiong F. 2019. Emerging artificial synaptic devices for neuromorphic computing. *Adv. Mater. Technol.* **4**, 1900037.
[45] Zhu J D, Zhang T, Yang Y C and Huang R. 2020. A comprehensive review on emerging artificial neuromorphic devices. *Appl. Phys. Rev.* **7**, 0113121
[46] Lu Q F, Sun F Q, Liu L, Li L H, Wang Y Y, Hao M M, Wang Z H, Wang S Q and Zhang T. 2020. Biological receptor-inspired flexible artificial synapse based on ionic dynamics. *Microsyst. Nanoeng.* **6**, 84.
[47] Han H, Yu H Y, Wei H H, Gong J D and Xu W T. 2019. Recent progress in three-terminal artificial synapses: from device to system. *Small* **15**, 1900695.
[48] Dai S L, Zhao Y W, Wang Y, Zhang J Y, Fang L, Jin S, Shao Y L and Huang J. 2019. Recent advances in transistor-based artificial synapses. *Adv. Funct. Mater.* **29**, 1903700.
[49] Huh W, Lee D and Lee C H. 2020. Memristors based on 2D materials as an artificial synapse for neuromorphic electronics. *Adv. Mater.* **32**, 2002092.
[50] Wang X M, Yang H H, Li E L, Cao C B, Zheng W, Chen H P and Li W W. 2023. Stretchable transistor-structured artificial synapses for neuromorphic electronics. *Small* **19**, 2205395.
[51] Choi S, Yang J and Wang G. 2020. Emerging memristive artificial synapses and neurons for energy-efficient neuromorphic computing. *Adv. Mater.* **32**, 2004659.
[52] Sun F Q, Lu Q F, Feng S M and Zhang T. 2021. Flexible artificial sensory systems based on neuromorphic devices. *ACS Nano* **15**, 3875–3899.
[53] Wang W S and Zhu L Q. 2023. Recent advances in neuromorphic transistors for artificial perception applications. *Sci. Technol. Adv. Mater.* **24**, 2152290.

[54] Ji X L, Zhao X Y, Tan M C and Zhao R. 2020. Artificial perception built on memristive system: visual, auditory, and tactile sensations. *Adv. Intell. Syst.* **2**, 1900118.
[55] Sarkar T, Lieberth K, Pavlou A, Frank T, Mailaender V, Mcculloch I, Blom P W M, Torricelli F and Gkoupidenis P. 2022. An organic artificial spiking neuron for *in situ* neuromorphic sensing and biointerfacing. *Nat. Electron.* **5**, 774–783.
[56] Donati E and Valle G. 2024. Neuromorphic hardware for somatosensory neuroprostheses. *Nat. Commun.* **15**, 556.
[57] Lee Y, Oh J Y and Lee T W. 2022. Neuromorphic skin based on emerging artificial synapses. *Adv. Mater. Technol.* **7**, 2200193.
[58] Wan C J, Cai P Q, Wang M, Qian Y, Huang W and Chen X D. 2020. Artificial sensory memory. *Adv. Mater.* **32**, 1902434.
[59] Chen S et al. 2024. Artificial organic afferent nerves enable closed-loop tactile feedback for intelligent robot. *Nat. Commun.* **15**, 7056.
[60] Liu W J, Du Z J, Duan Z Y, Li L and Shen G Z. 2024. Neuroprosthetic contact lens enabled sensorimotor system for point-of-care monitoring and feedback of intraocular pressure. *Nat. Commun.* **15**, 5635.
[61] Dalesio N M, Barreto Ortiz S F, Pluznick J L and Berkowitz D E. 2018. Olfactory, taste, and photo sensory receptors in non-sensory organs: it just makes sense. *Front. Physiol.* **9**, 1673.
[62] Svechtarova M I, Buzzacchera I, Toebes B J, Lauko J, Anton N and Wilson C J. 2016. Sensor devices inspired by the five senses: a review. *Electroanalysis* **28**, 1201–1241.
[63] Choi H, Kim Y, Kim S, Jung H, Lee S, Kim K, Han H S, Kim J Y, Shin M and Son D. 2023. Adhesive bioelectronics for sutureless epicardial interfacing. *Nat. Electron.* **6**, 779–789.
[64] Jin S B, Choi H, Seong D, You C L, Kang J S, Rho S, Lee W B, Son D and Shin M. 2023. Injectable tissue prosthesis for instantaneous closed-loop rehabilitation. *Nature* **623**, 58–65.
[65] Lee S et al. 2024. A shape-morphing cortex-adhesive sensor for closed-loop transcranial ultrasound neurostimulation. *Nat. Electron.* **7**, 800–814.
[66] Shin J H, Kwon J, Kim J U, Ryu H, Ok J, Joon Kwon S, Park H and Kim T I. 2022. Wearable EEG electronics for a brain–AI closed-loop system to enhance autonomous machine decision-making. *npj Flex. Electron.* **6**, 32.
[67] Giordano G F, Ferreira L F, Bezerra Í R S, Barbosa J A, Costa J N Y, Pimentel G J C and Lima R S. 2023. Machine learning toward high-performance electrochemical sensors. *Anal. Bioanal. Chem.* **415**, 3683–3692.
[68] Moin A et al. 2021. A wearable biosensing system with in-sensor adaptive machine learning for hand gesture recognition. *Nat. Electron.* **4**, 54–63.
[69] Wang M et al. 2020. Gesture recognition using a bioinspired learning architecture that integrates visual data with somatosensory data from stretchable sensors. *Nat. Electron.* **3**, 563–570.
[70] Han S, Kim T, Kim D, Park Y L and Jo S. 2018. Use of deep learning for characterization of microfluidic soft sensors. *IEEE Robot. Autom. Lett.* **3**, 873–880.
[71] Choi C et al. 2017. Human eye-inspired soft optoelectronic device using high-density MoS_2-graphene curved image sensor array. *Nat. Commun.* **8**, 1664.
[72] Kim J et al. 2014. Stretchable silicon nanoribbon electronics for skin prosthesis. *Nat. Commun.* **5**, 5747.
[73] Song J-K et al. 2022. Stretchable colour-sensitive quantum dot nanocomposites for shape-tunable multiplexed phototransistor arrays. *Nat. Nanotechnol.* **17**, 849–856.
[74] Lee J et al. 2024. Intelligent upper-limb exoskeleton integrated with soft bioelectronics and deep learning for intention-driven augmentation. *npj Flex. Electron.* **8**, 11.
[75] Luo Y F et al. 2023. Technology roadmap for flexible sensors. *ACS Nano* **17**, 5211–5295.
[76] Byun S H et al. 2019. Mechanically transformative electronics, sensors, and implantable devices. *Sci. Adv.* **5**, eaay0418.
[77] Xu C H, Yang Y R and Gao W. 2020. Skin-interfaced sensors in digital medicine: from materials to applications. *Matter* **2**, 1414–1445.
[78] Trung T Q and Lee N E. 2016. Flexible and stretchable physical sensor integrated platforms for wearable human-activity monitoringand personal healthcare. *Adv. Mater.* **28**, 4338–4372.
[79] Ray T R, Choi J, Bandodkar A J, Krishnan S, Gutruf P, Tian L M, Ghaffari R and Rogers J A. 2019. Bio-integrated wearable systems: a comprehensive review. *Chem. Rev.* **119**, 5461–5533.
[80] Lin M Y, Hu H J, Zhou S and Xu S. 2022. Soft wearable devices for deep-tissue sensing. *Nat. Rev. Mater.* **7**, 850–869.
[81] Jang K I et al. 2014. Rugged and breathable forms of stretchable electronics with adherent composite substrates for transcutaneous monitoring. *Nat. Commun.* **5**, 4779.
[82] Liu H Z, Li H G, Wang Z C, Wei X, Zhu H J, Sun M Z, Lin Y and Xu L Z. 2022. Robust and multifunctional kirigami electronics with a tough and permeable aramid nanofiber framework. *Adv. Mater.* **34**, 2207350.
[83] Kim J, Kim Y, Lee J, Shin M and Son D. 2023. Wearable liquid metal composite with skin-adhesive chitosan–alginate–chitosan hydrogel for stable electromyogram signal monitoring. *Polymers* **15**, 3692.
[84] Ho D H, Sun Q J, Kim S Y, Han J T, Kim D H and Cho J H. 2016. Stretchable and multimodal all graphene electronic skin. *Adv. Mater.* **28**, 2601–2608.
[85] Ho D H, Choi Y Y, Jo S B, Myoung J M and Cho J H. 2021. Sensing with MXenes: progress and prospects. *Adv. Mater.* **33**, 2005846.
[86] Lee H, Jang J, Lee J, Shin M, Lee J and Son D. 2023. Stretchable gold nanomembrane electrode with ionic hydrogel skin-adhesive properties. *Polymers* **15**, 3852.
[87] Gao W et al. 2016. Fully integrated wearable sensor arrays for multiplexed *in situ* perspiration analysis. *Nature* **529**, 509–514.
[88] Zeng Z K, Huang Z, Leng K M, Han W X, Niu H, Yu Y, Ling Q, Liu J H, Wu Z G and Zang J F. 2020. Nonintrusive monitoring of mental fatigue status using epidermal electronic systems and machine-learning algorithms. *ACS Sens.* **5**, 1305–1313.
[89] Sun T M et al. 2024. Artificial intelligence meets flexible sensors: emerging smart flexible sensing systems driven by machine learning and artificial synapses. *Nano-Micro Lett.* **16**, 14.
[90] Laib A, Terriche Y, Melit M, Su C L, Mutarraf M U, Bouchekara H R E H, Guerrero J M and Boudjefdjouf H. 2024. Enhanced artificial intelligence technique for soft fault localization and identification in complex aircraft microgrids. *Eng. Appl. Artif. Intell.* **127**, 107289.
[91] Yu C S, Yoo T, Kim H, Kim T T H, Chuan K C T and Kim B. 2021. A logic-compatible eDRAM compute-in-memory with embedded ADCs for processing neural networks. *IEEE Trans. Circuits Syst.* I **68**, 667–679.
[92] Xie S S, Ni C, Sayal A, Jain P, Hamzaoglu F and Kulkarni J P. 2021. 16.2 eDRAM-CIM: compute-in-memory design with reconfigurable embedded-dynamic-memory array realizing adaptive data converters and charge-domain computing. *In 2021 IEEE International Solid-State Circuits Conference*. (IEEE, San Francisco, CA, USA) pp 248–250.

[93] Zhang X Y and Basu A. 2023. A 915-1220 TOPS/W, 976-1301 GOPS hybrid in-memory computing based always-on image processing for neuromorphic vision sensors. *IEEE J. Solid-State Circuits* **58**, 589–599.
[94] Kim S, Kim S, Hong S, Kim S, Han D, Choi J and Yoo H J. 2024. C-DNN: an energy-efficient complementary deep-neural-network processor with heterogeneous CNN/SNN core architecture. *IEEE J. Solid-State Circuits* **59**, 157–172.
[95] Chen T R, Wang W J, Chen J Q, Fu H T, Yi W T, Cheng B J, Zhang H and Pan B. 2024. PipeCIM: a high-throughput computing-in-memory microprocessor with nested pipeline and RISC-V extended instructions. *IEEE Trans. Circuits Syst.* I **71**, 3214–3227.
[96] Yin G D et al. 2024. Cramming more weight data onto compute-in-memory macros for high task-level energy efficiency using custom ROM with 3984-kb/mm^2 density in 65-nm CMOS. *IEEE J. Solid-State Circuits* **59**, 1912–1925.
[97] Um S, Kim S, Hong S, Kim S and Yoo H J. 2024. LOG-CIM: an energy-efficient logarithmic quantization computing-in-memory processor with exponential parallel data mapping and zero-aware 6T Dual-WL cell. *IEEE J. Solid-State Circuits* **59**, 3330–3341.
[98] Qi X A, Li X T, Lou Y Q, Li Y F, Wang G X, Tang K T and Zhao J. 2024. A 0.67-to-5.4 TSOPs/W spiking neural network accelerator with 128/256 reconfigurable neurons and asynchronous fully connected synapses. *IEEE J. Solid-State Circuits* **59**, 3366–3377.
[99] Ju Y H, Wei Y J. and Gu J. 2024. A 65 nm general-purpose compute-in-memory processor supporting both general programming and deep learning tasks. *In IEEE J. Solid-State Circuits*. pp 1–12.
[100] Merolla P A et al. 2014. A million spiking-neuron integrated circuit with a scalable communication network and interface. *Science* **345**, 668–673.
[101] Davies M et al. 2018. Loihi: a neuromorphic manycore processor with on-chip learning. *IEEE Micro.* **38**, 82–99.
[102] Bankman D, Yang L T, Moons B, Verhelst M and Murmann B. 2019. An always-on 3.8 μ J/86% CIFAR-10 mixed-signal binary CNN processor with all memory on chip in 28-nm CMOS. *IEEE J. Solid-State Circuits* **54**, 158–172.
[103] Yin S H, Jiang Z W, Seo J S and Seok M. 2020. XNOR-SRAM: in-memory computing SRAM macro for binary/ternary deep neural networks. *IEEE J. Solid-State Circuits* **55**, 1733–1743.
[104] Pu J R, Goh W L, Nambiar V P, Wong M M and Do A T. 2021. A 5.28-mm^2 4.5-pJ/SOP energy-efficient spiking neural network hardware with reconfigurable high processing speed neuron core and congestion-aware router. *IEEE Trans. Circuits Syst.* I **68**, 5081–5094.
[105] Cao N Y, Chatterjee B, Liu J B, Cheng B Y, Gong M X, Chang M Y, Sen S and Raychowdhury A. 2022. A 65 nm wireless image SoC supporting on-chip DNN optimization and real-time computation-communication trade-off via actor-critical neuro-controller. *IEEE J. Solid-State Circuits* **57**, 2545–2559.
[106] Houshmand P et al. 2023. DIANA: an end-to-end hybrid DIgital and ANAlog neural network SoC for the edge. *IEEE J. Solid-State Circuits* **58**, 203–215.
[107] Sehgal R, Thareja T, Xie S S, Ni C and Kulkarni J P. 2023. A bit-serial, compute-in-SRAM design featuring hybrid-integrating ADCs and input dependent binary scaled precharge eliminating DACs for energy-efficient DNN inference. *IEEE J. Solid-State Circuits* **58**, 2109–2124.
[108] Wang H C, Liu R Z, Dorrance R, Dasalukunte D, Lake D and Carlton B. 2023. A charge domain SRAM compute-in-memory macro with C-2C ladder-based 8-bit MAC unit in 22-nm FinFET process for edge inference. *IEEE J. Solid-State Circuits* **58**, 1037–1050.
[109] Liu Y, Ma Y F, Shan N H, Zhao T H, Chen P Y and Wu M. 2024. 30.2 A 22nm 0.26nW/synapse spike-driven spiking neural network processing unit using time-step-first data-flow and sparsity-adaptive in-memory computing. *In 2024 IEEE International Solid-State Circuits Conference*. (IEEE, San Francisco, CA, USA) pp 484–486.
[110] Zhang J L, Huo D X, Zhang J, Qian C Q, Liu Q, Pan L Y, Wang Z H, Qiao N, Tang K T and Chen H. 2024. ANP-I: a 28-nm 1.5-pJ/SOP asynchronous spiking neural network processor enabling sub-0.1-μ J/sample on-chip learning for edge-AI applications. *IEEE J. Solid-State Circuits* **59**, 2717–2729.
[111] Zhao C Y et al. 2024. A 28-nm 36 Kb SRAM CIM engine with 0.173 μm^2 4T1T cell and self-load-0 weight update for AI inference and training applications. *IEEE J. Solid-State Circuits* **59**, 3277–3289.
[112] Zhong Y, Kuang Y S, Liu K F, Wang Z L, Feng S and Chen G. 2024. PAICORE: a 1.9-million-neuron 5.181-TSOPS/W digital neuromorphic processor with unified SNN-ANN and on-chip learning paradigm. *In IEEE J. Solid-State Circuits* pp 1–21.
[113] Kim D, She X Y, Rahman N M, Chekuri V C K and Mukhopadhyay S. 2020. Processing-in-memory-based on-chip learning with spike-time-dependent plasticity in 65-nm CMOS. *IEEE Solid-State Circuits Lett.* **3**, 278–281.
[114] Chen C Y, Dai Y S and Hong H C. 2024. A neuromorphic spiking neural network using time-to-first-spike coding scheme and analog computing in low-leakage 8T SRAM. *IEEE Trans. Very Large Scale Integr.* **32**, 848–859.
[115] Yao P, Wu H Q, Gao B, Tang J S, Zhang Q T, Zhang W Q, Yang J J and Qian H. 2020. Fully hardware-implemented memristor convolutional neural network. *Nature* **577**, 641–646.
[116] Wan W E et al. 2022. A compute-in-memory chip based on resistive random-access memory. *Nature* **608**, 504–512.
[117] Oh S, Shi Y H, Del Valle J, Salev P, Lu Y C, Huang Z S, Kalcheim Y, Schuller I K and Kuzum D. 2021. Energy-efficient Mott activation neuron for full-hardware implementation of neural networks. *Nat. Nanotechnol.* **16**, 680–687.
[118] Hung J M et al. 2021. A four-megabit compute-in-memory macro with eight-bit precision based on CMOS and resistive random-access memory for AI edge devices. *Nat. Electron.* **4**, 921–930.
[119] Jung S et al. 2022. A crossbar array of magnetoresistive memory devices for in-memory computing. *Nature* **601**, 211–216.
[120] Um M, Kang M, Kwak H, Noh K, Kim S and Lee H M. 2023. An ECRAM-based analog compute-in-memory neuromorphic system with high-precision current readout. *In 2023 IEEE Biomedical Circuits and Systems Conference*. (IEEE, Toronto, ON, Canada) pp 1–5.
[121] Ezzadeen M et al. 2024. Implementation of binarized neural networks immune to device variation and voltage drop employing resistive random access memory bridges and capacitive neurons. *Commun. Eng.* **3**, 80.
[122] Deaville P, Zhang B N and Verma N. 2024. A fully row/column-parallel in-memory computing macro in foundry MRAM with differential readout for noise rejection. *IEEE J. Solid-State Circuits* **59**, 2070–2080.
[123] Yan B N et al. 2019. RRAM-based spiking nonvolatile computing-in-memory processing engine with precision-configurable *in situ* nonlinear activation. *In 2019 Symposium on VLSI Technology*. (IEEE, Kyoto, Japan) pp T86–T87.
[124] Li W T, Sun X Y, Huang S S, Jiang H W and Yu S M. 2022. A 40-nm MLC-RRAM compute-in-memory macro with

sparsity control, on-chip write-verify, and temperature-independent ADC references. *IEEE J. Solid-State Circuits* **57**, 2868–2877.
[125] Li Y et al. 2023. An ADC-less RRAM-based computing-in-memory macro with binary CNN for efficient edge AI. *IEEE Trans. Circuits Syst.* II **70**, 1871–1875.
[126] Rao M Y et al. 2023. Thousands of conductance levels in memristors integrated on CMOS. *Nature* **615**, 823–829.
[127] Zhang W B et al. 2023. Edge learning using a fully integrated neuro-inspired memristor chip. *Science* **381**, 1205–1211.
[128] Jiang H et al. 2023. Multicore spiking neuromorphic chip in 180-nm with ReRAM synapses and digital neurons. *IEEE J. Emerg. Sel. Top Circuits Syst.* **13**, 975–985.
[129] Song W H et al. 2024. Programming memristor arrays with arbitrarily high precision for analog computing. *Science* **383**, 903–910.
[130] Hsu H H et al. 2024. A nonvolatile AI-edge processor with SLC–MLC hybrid ReRAM compute-in-memory macro using current–voltage-hybrid readout scheme. *IEEE J. Solid-State Circuits* **59**, 116–127.
[131] Wen T H et al. 2024. 34.8 A 22nm 16Mb floating-point ReRAM compute-in-memory macro with 31.2TFLOPS/W for AI edge devices. *In 2024 IEEE International Solid-State Circuits Conference*. (IEEE, San Francisco, CA, USA) pp 580–582.
[132] Wen T H et al. 2024. Fusion of memristor and digital compute-in-memory processing for energy-efficient edge computing. *Science* **384**, 325–332.
[133] Kang M J, Baeg K J, Khim D, Noh Y Y and Kim D Y. 2013. Printed, flexible, organic nano-floating-gate memory: effects of metal nanoparticles and blocking dielectrics on memory characteristics. *Adv. Funct. Mater.* **23**, 3503–3512.
[134] Qu T-Y et al. 2020. A flexible carbon nanotube sen-memory device. *Adv. Mater.* **32**, 1907288.
[135] Ren Y, Yang J Q, Zhou L, Mao J Y, Zhang S R, Zhou Y and Han S T. 2018. Gate-tunable synaptic plasticity through controlled polarity of charge trapping in fullerene composites. *Adv. Funct. Mater.* **28**, 1805599.
[136] Kim S, Choi B, Lim M, Yoon J, Lee J, Kim H D and Choi S J. 2017. Pattern recognition using carbon nanotube synaptic transistors with an adjustable weight update protocol. *ACS Nano* **11**, 2814–2822.
[137] Nam T U, Vo N T P, Jeong M W, Jung K H, Lee S H, Lee T I and Oh J Y. 2024. Intrinsically stretchable floating gate memory transistors for data storage of electronic skin devices. *ACS Nano* **18**, 14558–14568.
[138] Li M Z, Guo L C, Ding G L, Zhou K, Xiong Z Y, Han S T and Zhou Y. 2021. Inorganic perovskite quantum dot-based strain sensors for data storage and in-sensor computing. *ACS Appl. Mater. Interfaces* **13**, 30861–30873.
[139] Xiong X, Wang X, Hu Q L, Li X F and Wu Y Q. 2022. Flexible synaptic floating gate devices with dual electrical modulation based on ambipolar black phosphorus. *iScience* **25**, 103947.
[140] Li Q X et al. 2024. High-performance ferroelectric field-effect transistors with ultra-thin indium tin oxide channels for flexible and transparent electronics. *Nat. Commun.* **15**, 2686.
[141] Zhong G K et al. 2020. Flexible electronic synapse enabled by ferroelectric field effect transistor for robust neuromorphic computing. *Appl. Phys. Lett.* **117**, 092903.
[142] Jang S, Jang S, Lee E H, Kang M J, Wang G and Kim T W. 2019. Ultrathin conformable organic artificial synapse for wearable intelligent device applications. *ACS Appl. Mater. Interfaces* **11**, 1071–1080.
[143] Ren C L et al. 2020. Highly robust flexible ferroelectric field effect transistors operable at high temperature with low-power consumption. *Adv. Funct. Mater.* **30**, 1906131.
[144] Xiong L Q, Chen Y, Yu J, Xiong W M, Zhang X Y and Zheng Y. 2019. Stretchable ferroelectric field-effect-transistor with multi-level storage capacity and photo-modulated resistance. *Appl. Phys. Lett.* **115**, 153107.
[145] Joh H, Jung M, Hwang J, Goh Y, Jung T and Jeon S. 2022. Flexible ferroelectric hafnia-based synaptic transistor by focused-microwave annealing. *ACS Appl. Mater. Interfaces* **14**, 1326–1333.
[146] Yoon J, Kim J, Jung H, Cho J I, Park J H, Shin M, Kim I S, Kang J and Son D. 2024. Intrinsically stretchable sensory-neuromorphic system for sign language translation. *Curr. Opin. Solid State Mater. Sci.* **29**, 101142.
[147] Liu Y H, Zhu L Q, Feng P, Shi Y and Wan Q. 2015. Freestanding artificial synapses based on laterally proton-coupled transistors on chitosan membranes. *Adv. Mater.* **27**, 5599–5604.
[148] Van De Burgt Y, Lubberman E, Fuller E J, Keene S T, Faria G C, Agarwal S, Marinella M J, Alec Talin A and Salleo A. 2017. A non-volatile organic electrochemical device as a low-voltage artificial synapse for neuromorphic computing. *Nat. Mater.* **16**, 414–418.
[149] Nguyen T D, Trung T Q, Lee Y and Lee N E. 2022. Stretchable and stable electrolyte-gated organic electrochemical transistor synapse with a nafion membrane for enhanced synaptic properties. *Adv. Eng. Mater.* **24**, 2100918.
[150] Gao X X, Yin J, Zhu J, Chang J J, Zhang J C and Hao Y. 2024. Electrolyte-gated flexible MoS_2 synaptic transistors with short-term plasticity. *IEEE Electron Device Lett.* **45**, 605–608.
[151] Molina-Lopez F et al. 2019. Inkjet-printed stretchable and low voltage synaptic transistor array. *Nat. Commun.* **10**, 2676.
[152] Peng Y J, Gao L, Liu C J, Deng J Y, Xie M, Bai L B, Wang G, Cheng Y H, Huang W and Yu J S. 2023. Stretchable organic electrochemical transistors via three-dimensional porous elastic semiconducting films for artificial synaptic applications. *Nano Res.* **16**, 10206–10214.
[153] Li X H et al. 2023. 3D-printed intrinsically stretchable organic electrochemical synaptic transistor array. *ACS Appl. Mater. Interfaces* **15**, 41656–41665.
[154] Oh S, Cho J I, Lee B H, Seo S, Lee J H, Choo H, Heo K, Lee S Y and Park J H. 2021. Flexible artificial Si-In-Zn-O/ion gel synapse and its application to sensory-neuromorphic system for sign language translation. *Sci. Adv.* **7**, eabg9450.
[155] Shim H et al. 2019. Stretchable elastic synaptic transistors for neurologically integrated soft engineering systems. *Sci. Adv.* **5**, eaax4961.
[156] Pei J F et al. 2024. Scalable synaptic transistor memory from solution-processed carbon nanotubes for high-speed neuromorphic data processing. *Adv. Mater.* **37**, 2312783.
[157] Yu T F, Chen H Y, Liao M Y, Tien H C, Chang T T, Chueh C C and Lee W Y. 2020. Solution-processable anion-doped conjugated polymer for nonvolatile organic transistor memory with synaptic behaviors. *ACS Appl. Mater. Interfaces* **12**, 33968–33978.
[158] Yang Y T, Wu Y S, He W E, Tien H C, Yang W C, Michinobu T, Chen W C, Lee W Y and Chueh C C. 2022. Tuning ambipolarity of the conjugated polymer channel layers of floating-gate free transistors: from volatile memories to artificial synapses. *Adv. Sci.* **9**, 2203025.
[159] Wei P, Wang X D, Li X L, Han S Y, Qiao N, Zhang P, Deng Y F, Zhang W, Bu L J and Lu G H. 2021. Reconfigurable multifunctional ambipolar polymer-blend transistors with improved switching-off capability. *Adv. Funct. Mater.* **31**, 2103369.

[160] Wang Y et al. 2020. Modulation of binary neuroplasticity in a heterojunction-based ambipolar transistor. *ACS Appl. Mater. Interfaces* **12**, 15370–15379.
[161] Yu R J, Li E L, Wu X M, Yan Y J, He W X, He L H, Chen J W, Chen H P and Guo T L. 2020. Electret-based organic synaptic transistor for neuromorphic computing. *ACS Appl. Mater. Interfaces* **12**, 15446–15455.
[162] Yang W C, Lin Y C, Inagaki S, Shimizu H, Ercan E, Hsu L C, Chueh C C, Higashihara T and Chen W C. 2022. Low-energy-consumption and electret-free photosynaptic transistor utilizing poly (3-hexylthiophene)-based conjugated block copolymers. *Adv. Sci.* **9**, 2105190.
[163] Moon H et al. 2015. Synthesis of ultrathin polymer insulating layers by initiated chemical vapour deposition for low-power soft electronics. *Nat. Mater.* **14**, 628–635.
[164] Jang B C, Seong H, Kim S K, Kim J Y, Koo B J, Choi J, Yang S Y, Im S G and Choi S Y. 2016. Flexible nonvolatile polymer memory array on plastic substrate via initiated chemical vapor deposition. *ACS Appl. Mater. Interfaces* **8**, 12951–12958.
[165] Jang B C, Kim S, Yang S Y, Park J, Cha J H, Oh J, Choi J, Im S G, Dravid V P and Choi S Y. 2019. Polymer analog memristive synapse with atomic-scale conductive filament for flexible neuromorphic computing system. *Nano Lett.* **19**, 839–849.
[166] Yang M H, Zhao X L, Tang Q X, Cui N, Wang Z Q, Tong Y H and Liu Y C. 2018. Stretchable and conformable synapse memristors for wearable and implantable electronics. *Nanoscale* **10**, 18135–18144.
[167] Yi X H et al. 2019. Intrinsically stretchable resistive switching memory enabled by combining a liquid metal–based soft electrode and a metal–organic framework insulator. *Adv. Electron. Mater.* **5**, 1800655.
[168] Park J et al. 2022. Reversible electrical percolation in a stretchable and self-healable silver-gradient nanocomposite bilayer. *Nat. Commun.* **13**, 5233.
[169] Son D et al. 2014. Multifunctional wearable devices for diagnosis and therapy of movement disorders. *Nat. Nanotechnol.* **9**, 397–404.
[170] Sim K, Rao Z, Zou Z N, Ershad F, Lei J M, Thukral A, Chen J, Huang Q A, Xiao J L and Yu C J. 2019. Metal oxide semiconductor nanomembrane–based soft unnoticeable multifunctional electronics for wearable human-machine interfaces. *Sci. Adv.* **5**, eaav9653.
[171] Meng J L et al. 2021. *Flexible boron nitride-based memristor for in situ* digital and analogue neuromorphic computing applications. *Mater. Horiz.* **8**, 538–546.
[172] Bae H et al. 2019. Bioinspired polydopamine-based resistive-switching memory on cotton fabric for wearable neuromorphic device applications. *Adv. Mater. Technol.* **4**, 1900151.
[173] Kim S H et al. 2021. A bioinspired stretchable sensory-neuromorphic system. *Adv. Mater.* **33**, 2104690.
[174] Quiroga R Q, Reddy L, Kreiman G, Koch C and Fried I. 2005. Invariant visual representation by single neurons in the human brain. *Nature* **435**, 1102–1107.
[175] Wang G Z, Wang R B, Kong W Z and Zhang J H. 2018. Simulation of retinal ganglion cell response using fast independent component analysis. *Cogn. Neurodyn.* **12**, 615–624.
[176] Kumar D, Joharji L, Li H R, Rezk A, Nayfeh A and El-Atab N. 2023. Artificial visual perception neural system using a solution-processable MoS_2-based in-memory light sensor. *Light Sci. Appl.* **12**, 109.
[177] Han C, Han X W, Han J Y, He M Y, Peng S L, Zhang C Y, Liu X C, Gou J and Wang J. 2022. Light-stimulated synaptic transistor with high PPF feature for artificial visual perception system application. *Adv. Funct. Mater.* **32**, 2113053.
[178] He J Q, Wei R L, Ge S P, Wu W Q, Guo J C, Tao J, Wang R, Wang C F and Pan C F. 2024. Artificial visual-tactile perception array for enhanced memory and neuromorphic computations. *InfoMat* **6**, e12493.
[179] Cao Y X et al. 2023. Neuromorphic visual artificial synapse in-memory computing systems based on GeO_x-coated MXene nanosheets. *Nano Energy* **112**, 108441.
[180] Lee Y et al. 2018. Stretchable organic optoelectronic sensorimotor synapse. *Sci. Adv.* **4**, eaat7387.
[181] Ni Y, Liu J Q, Han H, Yu Q B, Yang L, Xu Z, Jiang C, Liu L and Xu W. 2024. Visualized in-sensor computing. *Nat. Commun.* **15**, 3454.
[182] Bao H et al. 2022. Toward memristive in-memory computing: principles and applications. *Front. Optoelectron.* **15**, 23.
[183] Ren Q Q, Zhu C Y, Ma S J, Wang Z Q, Yan J M, Wan T Q, Yan W C and Chai Y. 2024. Optoelectronic devices for in-sensor computing. *Adv. Mater.* 2407476.
[184] Meng J L, Wang T Y, Zhu H, Ji L, Bao W Z, Zhou P, Chen L, Sun Q Q and Zhang D W. 2022. Integrated in-sensor computing optoelectronic device for environment-adaptable artificial retina perception application. *Nano Lett.* **22**, 81–89.
[185] Kwon S M, Cho S W, Kim M, Heo J S, Kim Y H and Park S K. 2019. Environment-adaptable artificial visual perception behaviors using a light-adjustable optoelectronic neuromorphic device array. *Adv. Mater.* **31**, 1906433.
[186] Kwon S M et al. 2021. Large-area pixelized optoelectronic neuromorphic devices with multispectral light-modulated bidirectional synaptic circuits. *Adv. Mater.* **33**, 2105017.
[187] Seo S et al. 2018. Artificial optic-neural synapse for colored and color-mixed pattern recognition. *Nat. Commun.* **9**, 5106.
[188] Wang C Y et al. 2024. Strain-insensitive viscoelastic perovskite film for intrinsically stretchable neuromorphic vision-adaptive transistors. *Nat. Commun.* **15**, 3123.
[189] Wang H L et al. 2018. A ferroelectric/electrochemical modulated organic synapse for ultraflexible, artificial visual-perception system. *Adv. Mater.* **30**, 1803961.
[190] Chen S, Lou Z, Chen D and Shen G Z. 2018. An artificial flexible visual memory system based on an UV-motivated memristor. *Adv. Mater.* **30**, 1705400.
[191] Xie T H et al. 2023. Carbon nanotube optoelectronic synapse transistor arrays with ultra-low power consumption for stretchable neuromorphic vision systems. *Adv. Funct. Mater.* **33**, 2303970.
[192] Xu F, Zhang C, Zhao X L, Yu H Y, Zhao G D, Li J T, Wang B, Tong Y H, Tang Q X and Liu Y C. 2022. Intrinsically stretchable photonic synaptic transistors for retina-like visual image systems. *J. Mater. Chem.* C **10**, 10586–10594.
[193] Shi J L, Jie J S, Deng W, Luo G, Fang X C, Xiao Y L, Zhang Y J, Zhang X J and Zhang X H. 2022. A fully solution-printed photosynaptic transistor array with ultralow energy consumption for artificial-vision neural networks. *Adv. Mater.* **34**, 2200380.
[194] Liao F Y et al. 2022. Bioinspired in-sensor visual adaptation for accurate perception. *Nat. Electron.* **5**, 84–91.
[195] Jo C, Kim J, Kwak J Y, Kwon S M, Park J B, Kim J, Park G S, Kim M G, Kim Y H and Park S K. 2022. Retina-inspired color-cognitive learning via chromatically controllable mixed quantum dot synaptic transistor arrays. *Adv. Mater.* **34**, 2108979.
[196] Liu W R, Chen W Z, Jin C X, Xu Y C, Shi X F, He B, Peng Y Y, Yang J L and Sun J. 2023. Organic optoelectrical synaptic transistors for color information processing. *Appl. Phys. Lett.* **123**, 193703.
[197] Choi C, Seung H and Kim D H. 2022. Bio-inspired electronic eyes and synaptic photodetectors for mobile artificial vision. *IEEE J. Flex. Electron.* **1**, 76–87.

[198] Zhang K et al. 2017. Origami silicon optoelectronics for hemispherical electronic eye systems. *Nat. Commun.* **8**, 1782.
[199] Wang M, Luo Y F, Wang T, Wan C J, Pan L, Pan S W, He K, Neo A and Chen X D. 2021. Artificial skin perception. *Adv. Mater.* **33**, 2003014.
[200] Sundaram S, Kellnhofer P, Li Y Z, Zhu J Y, Torralba A and Matusik W. 2019. Learning the signatures of the human grasp using a scalable tactile glove. *Nature* **569**, 698–702.
[201] Yu H B et al. 2024. Skin-inspired capacitive flexible tactile sensor with an asymmetric structure for detecting directional shear forces. *Adv. Sci.* **11**, 2305883.
[202] Lv C Y, Tian C C, Jiang J S, Dang Y, Liu Y, Duan X X, Li Q N, Chen X J and Xie M Y. 2023. Ultrasensitive linear capacitive pressure sensor with wrinkled microstructures for tactile perception. *Adv. Sci.* **10**, 2206807.
[203] Huang X D, Ma Z Y, Xia W T, Hao L X, Wu Y H, Lu S, Luo Y S, Qin L G and Dong G N. 2024. A high-sensitivity flexible piezoelectric tactile sensor utilizing an innovative rigid-in-soft structure. *Nano Energy* **129**, 110019.
[204] Zhang J H et al. 2022. Finger-inspired rigid-soft hybrid tactile sensor with superior sensitivity at high frequency. *Nat. Commun.* **13**, 5076.
[205] Chen Y H et al. 2019. Piezotronic graphene artificial sensory synapse. *Adv. Funct. Mater.* **29**, 1900959.
[206] Sun F Q, Lu Q F, Hao M M, Wu Y, Li Y, Liu L, Li L H, Wang Y Y and Zhang T. 2022. An artificial neuromorphic somatosensory system with spatio-temporal tactile perception and feedback functions. *npj Flex. Electron.* **6**, 72.
[207] Wan C J et al. 2018. An artificial sensory neuron with tactile perceptual learning. *Adv. Mater.* **30**, 1801291.
[208] Tan H W, Tao Q Z, Pande I, Majumdar S, Liu F, Zhou Y F, Persson P O Å, Rosen J and Van Dijken S. 2020. Tactile sensory coding and learning with bio-inspired optoelectronic spiking afferent nerves. *Nat. Commun.* **11**, 1369.
[209] Jiang C P, Liu J Q, Yang L, Gong J D, Wei H H and Xu W T. 2022. A flexible artificial sensory nerve enabled by nanoparticle-assembled synaptic devices for neuromorphic tactile recognition. *Adv. Sci.* **9**, 2106124.
[210] Zeng J H, Chen L B, Bu T Z, Wang Z Y, Gong L K, Zhang Z B, Zhao J Q, Lin Wang Z and Zhang C. 2024. Intrinsically stretchable tribotronic mechanoplastic artificial synapse. *Chem. Eng. J.* **492**, 152412.
[211] Song Z W et al. 2022. A flexible triboelectric tactile sensor for simultaneous material and texture recognition. *Nano Energy* **93**, 106798.
[212] Cheng Y, Wu D, Hao S F, Jie Y, Cao X, Wang N and Wang Z L. 2019. Highly stretchable triboelectric tactile sensor for electronic skin. *Nano Energy* **64**, 103907.
[213] Lee Y R, Trung T Q, Hwang B U and Lee N E. 2020. A flexible artificial intrinsic-synaptic tactile sensory organ. *Nat. Commun.* **11**, 2753.
[214] Lee Y et al. 2018. Flexible ferroelectric sensors with ultrahigh pressure sensitivity and linear response over exceptionally broad pressure range. *ACS Nano* **12**, 4045–4054.
[215] Huynh H Q, Trung T Q, Bag A, Do T D, Sultan M J, Kim M and Lee N E. 2023. Bio-inspired artificial fast-adaptive and slow-adaptive mechanoreceptors with synapse-like functions. *Adv. Funct. Mater.* **33**, 2303535.
[216] Kim Y et al. 2018. A bioinspired flexible organic artificial afferent nerve. *Science* **360**, 998–1003.
[217] Wu M G et al. 2023. Stretchable, skin-conformable neuromorphic system for tactile sensory recognizing and encoding. *InfoMat* **5**, e12472.
[218] Chun S et al. 2021. An artificial neural tactile sensing system. *Nat. Electron.* **4**, 429–438.
[219] Sundaram S. 2020. How to improve robotic touch. *Science* **370**, 768–769.
[220] Tee B C K et al. 2015. A skin-inspired organic digital mechanoreceptor. *Science* **350**, 313–316.
[221] Kang J et al. 2018. Tough and water-insensitive self-healing elastomer for robust electronic skin. *Adv. Mater.* **30**, 1706846.
[222] Kim S H et al. 2019. An ultrastretchable and self-healable nanocomposite conductor enabled by autonomously percolative electrical pathways. *ACS Nano* **13**, 6531–6539.
[223] Wang L L, Jackman J A, Park J H, Tan E L and Cho N J. 2017. A flexible, ultra-sensitive chemical sensor with 3D biomimetic templating for diabetes-related acetone detection. *J. Mater. Chem.* B **5**, 4019–4024.
[224] Duy L T, Trung T Q, Hanif A, Siddiqui S, Roh E, Lee W and Lee N E. 2017. A stretchable and highly sensitive chemical sensor using multilayered network of polyurethane nanofibres with self-assembled reduced graphene oxide. *2D Mater.* **4**, 025062.
[225] Li H Y, Lee C S, Kim D H and Lee J H. 2018. Flexible room-temperature NH_3 sensor for ultrasensitive, selective, and humidity-independent gas detection. *ACS Appl. Mater. Interfaces* **10**, 27858–27867.
[226] Tang N, Zhou C, Xu L H, Jiang Y, Qu H M and Duan X X. 2019. A fully integrated wireless flexible ammonia sensor fabricated by soft nano-lithography. *ACS Sens.* **4**, 726–732.
[227] Punetha D, Kar M and Pandey S K. 2020. A new type low-cost, flexible and wearable tertiary nanocomposite sensor for room temperature hydrogen gas sensing. *Sci. Rep.* **10**, 2151.
[228] Wu Q W, Shen W F, Lv D W, Chen W G, Song W J and Tan R Q. 2021. An enhanced flexible room temperature ammonia gas sensor based on GP-PANI/PVDF multihierarchical nanocomposite film. *Sens. Actuators* B **334**, 129630.
[229] Moon D B, Bag A, Lee H B, Meeseepong M, Lee D H and Lee N E. 2021. A stretchable, room-temperature operable, chemiresistive gas sensor using nanohybrids of reduced graphene oxide and zinc oxide nanorods. *Sens. Actuators* B **345**, 130373.
[230] Zhang F Z, Lin Q J, Han F, Wang Z W, Tian B, Zhao L B, Dong T and Jiang Z D. 2022. A flexible and wearable NO_2 gas detection and early warning device based on a spraying process and an interdigital electrode at room temperature. *Microsyst. Nanoeng.* **8**, 40.
[231] Yang L et al. 2022. Moisture-resistant, stretchable NO_x gas sensors based on laser-induced graphene for environmental monitoring and breath analysis. *Microsyst. Nanoeng.* **8**, 78.
[232] Lim H, Kwon H, Kang H, Jang J E and Kwon H J. 2023. Semiconducting MOFs on ultraviolet laser-induced graphene with a hierarchical pore architecture for NO_2 monitoring. *Nat. Commun.* **14**, 3114.
[233] Zhao G D, Sun J, Zhang M X, Guo S L, Wang X, Li J T, Tong Y H, Zhao X L, Tang Q X and Liu Y C. 2023. Highly strain-stable intrinsically stretchable olfactory sensors for imperceptible health monitoring. *Adv. Sci.* **10**, 2302974.
[234] Wang T, Huang H M, Wang X X and Guo X. 2021. An artificial olfactory inference system based on memristive devices. *InfoMat* **3**, 804–813.
[235] Ban C Y et al. 2021. An artificial olfactory memory system for monitoring and recording of volatile organic compounds. *Adv. Mater. Technol.* **6**, 2100366.
[236] Li J, Fu W H, Lei Y X, Li L K, Zhu W Q and Zhang J H. 2022. Oxygen-vacancy-induced synaptic plasticity in an electrospun InGdO nanofiber transistor for a gas sensory system with a learning function. *ACS Appl. Mater. Interfaces* **14**, 8587–8597.
[237] Han J K, Kang M G, Jeong J, Cho I, Yu J M, Yoon K J, Park I and Choi Y K. 2022. Artificial olfactory neuron for an in-sensor neuromorphic nose. *Adv. Sci.* **9**, 2106017.

[238] Song H W, Moon D, Won Y, Cha Y K, Yoo J, Park T H and Oh J H. 2024. A pattern recognition artificial olfactory system based on human olfactory receptors and organic synaptic devices. *Sci. Adv.* **10**, eadl2882.
[239] Dong L Y, Xue B J, Wei G D, Yuan S, Chen M, Liu Y, Su Y, Niu Y, Xu B S and Wang P. 2024. Highly promising 2D/1D BP-C/CNT bionic opto-olfactory co-sensory artificial synapses for multisensory integration. *Adv. Sci.* **11**, 2403665.
[240] Song Z Q, Tong Y H, Zhao X L, Ren H, Tang Q X and Liu Y C. 2019. A flexible conformable artificial organ-damage memory system towards hazardous gas leakage based on a single organic transistor. *Mater. Horiz.* **6**, 717–726.
[241] Chouhdry H H, Lee D H, Bag A and Lee N E. 2023. A flexible artificial chemosensory neuronal synapse based on chemoreceptive ionogel-gated electrochemical transistor. *Nat. Commun.* **14**, 821.
[242] Deng Y P et al. 2023. A Flexible and biomimetic olfactory synapse with gasotransmitter-mediated plasticity. *Adv. Funct. Mater.* **33**, 2214139.
[243] Zollo L et al. 2019. Restoring tactile sensations via neural interfaces for real-time force-and-slippage closed-loop control of bionic hands. *Sci. Robot.* **4**, eaau9924.
[244] Clites T R, Carty M J, Ullauri J B, Carney M E, Mooney L M, Duval J F, Srinivasan S S and Herr H M. 2018. Proprioception from a neurally controlled lower-extremity prosthesis. *Sci. Transl. Med.* **10**, eaap8373.
[245] Wang W C et al. 2023. Neuromorphic sensorimotor loop embodied by monolithically integrated, low-voltage, soft e-skin. *Science* **380**, 735–742.
[246] Ortiz-Catalan M, Håkansson B and Brånemark R. 2014. An osseointegrated human-machine gateway for long-term sensory feedback and motor control of artificial limbs. *Sci. Transl. Med.* **6**, 257re6.
[247] Wenger N, Moraud E M, Raspopovic S, Bonizzato M, DiGiovanna J, Musienko P, Morari M, Micera S and Courtine G. 2014. Closed-loop neuromodulation of spinal sensorimotor circuits controls refined locomotion after complete spinal cord injury. *Sci. Transl. Med.* **6**, 255ra133.
[248] Wagner F B et al. 2018. Targeted neurotechnology restores walking in humans with spinal cord injury. *Nature* **563**, 65–71.
[249] D'Anna E et al. 2019. A closed-loop hand prosthesis with simultaneous intraneural tactile and position feedback. *Sci. Robot.* **4**, eaau8892.
[250] George J A et al. 2019. Biomimetic sensory feedback through peripheral nerve stimulation improves dexterous use of a bionic hand. *Sci. Robot.* **4**, eaax2352.
[251] Petrini F M et al. 2019. Sensory feedback restoration in leg amputees improves walking speed, metabolic cost and phantom pain. *Nat. Med.* **25**, 1356–1363.
[252] Vu P P et al. 2020. A regenerative peripheral nerve interface allows real-time control of an artificial hand in upper limb amputees. *Sci. Transl. Med.* **12**, eaay2857.
[253] Oh H, Yi G C, Yip M and Dayeh S A. 2020. Scalable tactile sensor arrays on flexible substrates with high spatiotemporal resolution enabling slip and grip for closed-loop robotics. *Sci. Adv.* **6**, eabd7795.
[254] Bonizzato M and Martinez M. 2021. An intracortical neuroprosthesis immediately alleviates walking deficits and improves recovery of leg control after spinal cord injury. *Sci. Transl. Med.* **13**, eabb4422.
[255] Rowald A et al. 2022. Activity-dependent spinal cord neuromodulation rapidly restores trunk and leg motor functions after complete paralysis. *Nat. Med.* **28**, 260–271.
[256] Kathe C et al. 2022. The neurons that restore walking after paralysis. *Nature* **611**, 540–547.
[257] Gu G Y et al. 2023. A soft neuroprosthetic hand providing simultaneous myoelectric control and tactile feedback. *Nat. Biomed. Eng.* **7**, 589–598.
[258] Lorach H et al. 2023. Walking naturally after spinal cord injury using a brain–spine interface. *Nature* **618**, 126–133.
[259] Milekovic T et al. 2023. A spinal cord neuroprosthesis for locomotor deficits due to Parkinson's disease. *Nat. Med.* **29**, 2854–2865.
[260] Ortiz-Catalan M et al. 2023. A highly integrated bionic hand with neural control and feedback for use in daily life. *Sci. Robot.* **8**, eadf7360.
[261] Nanivadekar A C et al. 2024. Restoration of sensory feedback from the foot and reduction of phantom limb pain via closed-loop spinal cord stimulation. *Nat. Biomed. Eng.* **8**, 992–1003.
[262] Osborn L E et al. 2024. Evoking natural thermal perceptions using a thin-film thermoelectric device with high cooling power density and speed. *Nat. Biomed. Eng.* **8**, 1004–1017.
[263] Valle G et al. 2024. Biomimetic computer-to-brain communication enhancing naturalistic touch sensations via peripheral nerve stimulation. *Nat. Commun.* **15**, 1151.
[264] Song H et al. 2024. Continuous neural control of a bionic limb restores biomimetic gait after amputation. *Nat. Med.* **30**, 2010–2019.
[265] Park S I et al. 2015. Soft, stretchable, fully implantable miniaturized optoelectronic systems for wireless optogenetics. *Nat. Biotechnol.* **33**, 1280–1286.
[266] Koo J et al. 2018. Wireless bioresorbable electronic system enables sustained nonpharmacological neuroregenerative therapy. *Nat. Med.* **24**, 1830–1836.
[267] Liu Y X et al. 2019. Soft and elastic hydrogel-based microelectronics for localized low-voltage neuromodulation. *Nat. Biomed. Eng.* **3**, 58–68.
[268] Zhang Y et al. 2019. Battery-free, fully implantable optofluidic cuff system for wireless optogenetic and pharmacological neuromodulation of peripheral nerves. *Sci. Adv.* **5**, eaaw5296.
[269] Liu Y X et al. 2020. Morphing electronics enable neuromodulation in growing tissue. *Nat. Biotechnol.* **38**, 1031–1036.
[270] Song K I et al. 2020. Adaptive self-healing electronic epineurium for chronic bidirectional neural interfaces. *Nat. Commun.* **11**, 4195.
[271] Choi Y S et al. 2020. Stretchable, dynamic covalent polymers for soft, long-lived bioresorbable electronic stimulators designed to facilitate neuromuscular regeneration. *Nat. Commun.* **11**, 5990.
[272] Seo H et al. 2021. Durable and fatigue-resistant soft peripheral neuroprosthetics for *in vivo* bidirectional signaling. *Adv. Mater.* **33**, 2007346.
[273] Reeder J T et al. 2022. Soft, bioresorbable coolers for reversible conduction block of peripheral nerves. *Science* **377**, 109–115.
[274] Lee G et al. 2022. A bioresorbable peripheral nerve stimulator for electronic pain block. *Sci. Adv.* **8**, eabp9169.
[275] Zhao Y C et al. 2022. Soft strain-insensitive bioelectronics featuring brittle materials. *Science* **378**, 1222–1227.
[276] Jiang Y et al. 2023. A universal interface for plug-and-play assembly of stretchable devices. *Nature* **614**, 456–462.
[277] Strakosas X et al. 2023. Metabolite-induced *in vivo* fabrication of substrate-free organic bioelectronics. *Science* **379**, 795–802.
[278] Rochford A E et al. 2023. Functional neurological restoration of amputated peripheral nerve using biohybrid regenerative bioelectronics. *Sci. Adv.* **9**, eadd8162.
[279] Zhou W J L et al. 2023. Soft and stretchable organic bioelectronics for continuous intraoperative neurophysiological monitoring during microsurgery. *Nat. Biomed. Eng.* **7**, 1270–1281.

[280] Yi J Q et al. 2023. Water-responsive supercontractile polymer films for bioelectronic interfaces. *Nature* **624**, 295–302.
[281] Seong D et al. 2024. Sticky and strain-gradient artificial epineurium for sutureless nerve repair in rodents and nonhuman primates. *Adv. Mater.* **36**, 2307810.
[282] Sun P C et al. 2024. A biodegradable and flexible neural interface for transdermal optoelectronic modulation and regeneration of peripheral nerves. *Nat. Commun.* **15**, 4721.
[283] Liu F Y, Deswal S, Christou A, Shojaei Baghini M, Chirila R, Duval J F, Srinivasan S S and Herr H M. 2022. Printed synaptic transistor–based electronic skin for robots to feel and learn. *Sci. Robot.* **7**, eabl7286.
[284] Lee Y et al. 2023. A low-power stretchable neuromorphic nerve with proprioceptive feedback. *Nat. Biomed. Eng.* **7**, 511–519.
[285] Chen L B, Karilanova S, Chaki S, Wen C Y, Wang L S, Winblad B, Zhang S L, Özçelikkale A and Zhang Z B. 2024. Spike timing–based coding in neuromimetic tactile system enables dynamic object classification. *Science* **384**, 660–665.
[286] Seo D G et al. 2019. Versatile neuromorphic electronics by modulating synaptic decay of single organic synaptic transistor: from artificial neural networks to neuro-prosthetics. *Nano Energy* **65**, 104035.
[287] Liu Y Q, Li E L, Wang X M, Chen Q Z, Zhou Y L, Hu Y Y, Chen G X, Chen H P and Guo T L. 2020. Self-powered artificial auditory pathway for intelligent neuromorphic computing and sound detection. *Nano Energy* **78**, 105403.
[288] Yun S Y, Han J K, Lee S W, Yu J M, Jeon S B and Choi Y K. 2023. Self-aware artificial auditory neuron with a triboelectric sensor for spike-based neuromorphic hardware. *Nano Energy* **109**, 108322.
[289] Yang L, Wang Z X, Zhang S, Li Y, Jiang C P, Sun L and Xu W T. 2023. Neuromorphic gustatory system with salt-taste perception, information processing, and excessive-intake warning capabilities. *Nano Lett.* **23**, 8–16.
[290] Ghosh S, Pannone A, Sen D, Wali A, Ravichandran H and Das S. 2023. An all 2D bio-inspired gustatory circuit for mimicking physiology and psychology of feeding behavior. *Nat. Commun.* **14**, 6021.
[291] Liu G C, Wen W, Zhao Z Y, Huang X, Li Y F, Qin M C, Pan Z C, Guo Y L and Liu Y Q. 2023. Bionic tactile-gustatory receptor for object identification based on all-polymer electrochemical transistor. *Adv. Mater.* **35**, 2300242.
[292] He Y F, Ge Z L, Li Z Y, Li Z X, Liu R P, Zhang L M, Lan L Y, Yue W and Xie Z. 2024. All-polymer organic electrochemical synaptic transistor with controlled ionic dynamics for high-performance wearable and sustainable reservoir computing. *Adv. Funct. Mater*. **35** 2415595.
[293] Yu J R, Yang X X, Gao G Y, Xiong Y, Wang Y F, Han J, Chen Y H, Zhang H, Sun Q J and Wang Z L. 2021. Bioinspired mechano-photonic artificial synapse based on graphene/MoS_2 heterostructure. *Sci. Adv.* **7**, eabd9117.
[294] Wu X M, Li E L, Liu Y Q, Lin W K, Yu R J, Chen G X, Hu Y Y, Chen H P and Guo T L. 2021. Artificial multisensory integration nervous system with haptic and iconic perception behaviors. *Nano Energy* **85**, 106000.
[295] Lee H R, Lee D and Oh J H. 2021. A hippocampus-inspired dual-gated organic artificial synapse for simultaneous sensing of a neurotransmitter and light. *Adv. Mater.* **33**, 2100119.
[296] Liu M W et al. 2022. A star-nose-like tactile-olfactory bionic sensing array for robust object recognition in non-visual environments. *Nat. Commun.* **13**, 79.
[297] Li P Z et al. 2024. Reconfigurable optoelectronic transistors for multimodal recognition. *Nat. Commun.* **15**, 3257.
[298] Tan D C, Zhang Z R, Shi H H, Sun N, Li Q K, Bi S, Huang J J, Liu Y H, Guo Q L and Jiang C M. 2024. Bioinspired artificial visual-respiratory synapse as multimodal scene recognition system with oxidized-vacancies MXene. *Adv. Mater.* **36**, 2407751.
[299] Chen H M, Shan L T, Gao C S, Chen C, Liu D, Chen H P, Guo T L and Hu W P. 2024. Artificial multisensory system with optical feedback for multimodal perceptual imaging. *Chem. Eng. J.* **487**, 150542.
[300] Zhu M L, Sun Z D and Lee C. 2022. Soft modular glove with multimodal sensing and augmented haptic feedback enabled by materials' multifunctionalities. *ACS Nano* **16**, 14097–14110.
[301] Wan H C, Zhao J Y, Lo L W, Cao Y Q, Sepulveda N and Wang C. 2021. Multimodal artificial neurological sensory–memory system based on flexible carbon nanotube synaptic transistor. *ACS Nano* **15**, 14587–14597.
[302] Jiang C P, Xu H H, Yang L, Liu J Q, Li Y, Takei K and Xu W T. 2024. Neuromorphic antennal sensory system. *Nat. Commun.* **15**, 2109.
[303] Kim Y, Lee K, Lee J, Jang S, Kim H, Lee H, Lee S W, Wang G and Park C. 2021. Bird-inspired self-navigating artificial synaptic compass. *ACS Nano* **15**, 20116–20126.
[304] Zheng Y K, Ghosh S and Das S. 2024. A butterfly-inspired multisensory neuromorphic platform for integration of visual and chemical cues. *Adv. Mater.* **36**, 2307380.
[305] Wang Y, Gong Y, Huang S M, Xing X C, Lv Z Y, Wang J J, Yang J Q, Zhang G H, Zhou Y and Han S T. 2021. Memristor-based biomimetic compound eye for real-time collision detection. *Nat. Commun.* **12**, 5979.
[306] Trung T Q and Lee N E. 2017. Recent progress on stretchable electronic devices with intrinsically stretchable components. *Adv. Mater.* **29**, 1603167.
[307] Huang X Y, Wang L, Wang H C, Zhang B Z, Wang X B, Stening R Y Z, Sheng X and Yin L. 2020. Materials strategies and device architectures of emerging power supply devices for implantable bioelectronics. *Small* **16**, 1902827.
[308] Dargusch M, Liu W D and Chen Z G. 2020. Thermoelectric generators: alternative power supply for wearable electrocardiographic systems. *Adv. Sci.* **7**, 2001362.
[309] Zhang W J, Wang X C, Duan J, Zheng Z F, Zhang J, Hang G G and Liu Z. 2024. Recent research advances in textile-based flexible power supplies and displays for smart wearable applications. *ACS Appl. Electron. Mater.* **6**, 5429–5455.
[310] Ouyang W et al. 2023. A wireless and battery-less implant for multimodal closed-loop neuromodulation in small animals. *Nat. Biomed. Eng.* **7**, 1252–1269.
[311] Gutruf P et al. 2019. Wireless, battery-free, fully implantable multimodal and multisite pacemakers for applications in small animal models. *Nat. Commun.* **10**, 5742.
[312] Niu S M et al. 2019. A wireless body area sensor network based on stretchable passive tags. *Nat. Electron.* **2**, 361–368.